Max-Planck-Institut für Meteorologie

REPORT No. 320

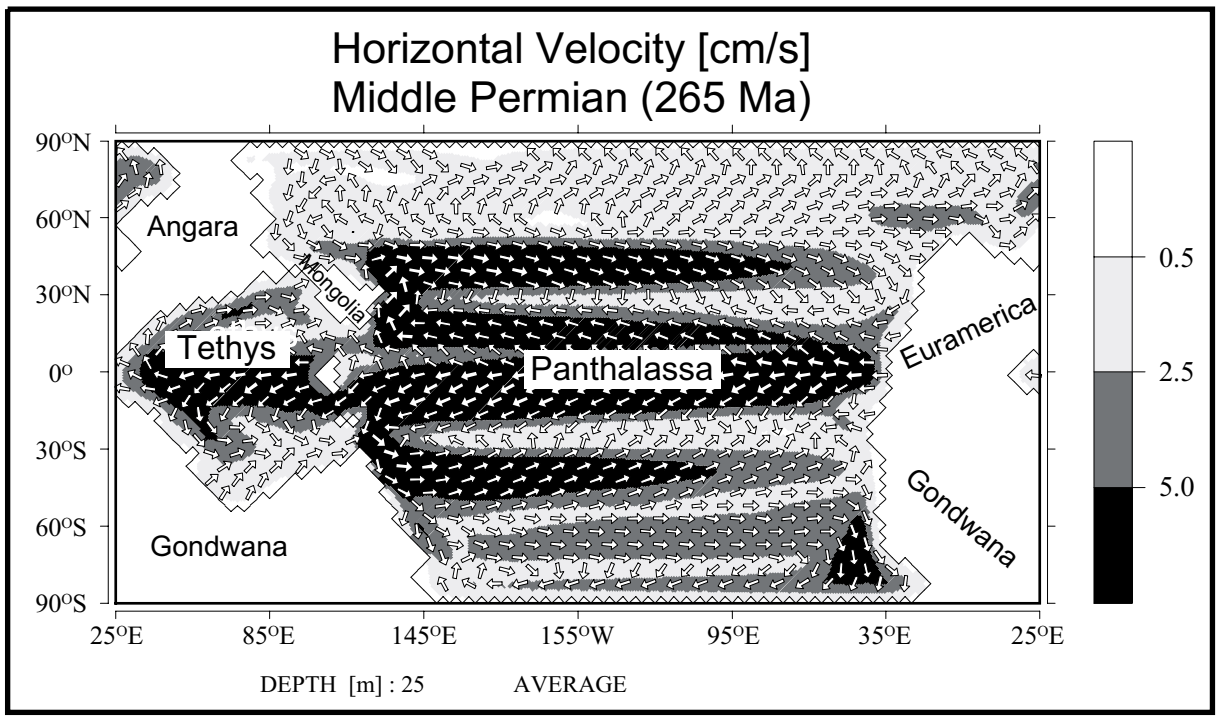

SIMULATED WARM POLAR CURRENTS DURING THE MIDDLE PERMIAN

by

A. M. E. WINGUTH • C. HEINZE • J.E. KUTZBACH • E. MAIER-REIMER
U. MIKOLAJEWICZ • D. ROWLEY • A. REES • A. M. ZIEGLER

HAMBURG, May 2001

AUTHORS:

Christoph Heinze
Ernst Maier-Reimer
Uwe Mikolajewicz

Max-Planck-Institut
für Meteorologie

Arne M. E. Winguth
John E. Kutzbach

Center for Climatic Research,
University of Wisconsin,
1225 W. Dayton St.,
Madison,
WI 53706
U.S.A.

David Rowley
Allister Rees
Alfred M. Ziegler

Department of Geophysical Sciences,
University of Chicago,
5734 S. Ellis Av.,
Chicago,
IL 60637
U.S.A.

MAX-PLANCK-INSTITUT
FÜR METEOROLOGIE
BUNDESSTRASSE 55
D - 20146 HAMBURG
GERMANY

Tel.: +49-(0)40-4 11 73-0
Telefax: +49-(0)40-4 11 73-298
E-Mail: <name> @ dkrz.de

Simulated Warm Polar Currents during the Middle Permian

A. M. E. Winguth[1], C. Heinze[3], J. E. Kutzbach[1], E. Maier-Reimer[3], U. Mikolajewicz[3], D. Rowley[2], A. Rees[2], and A.M. Ziegler[2]

[1]Center for Climatic Research, University of Wisconsin, Madison, Wisconsin.
[2]Department of Geophysical Sciences, University of Chicago, Illinois.
[3]Max-Planck-Institut fuer Meteorologie, Hamburg, Germany.

Abstract

During Permian Stage 6 (Wordian, Kazanian) the Pangaean supercontinent was surrounded by a superocean - Panthalassa. An ocean general circulation model has been coupled to an atmospheric energy balance model to simulate the sensitivity of the Wordian climate (~265 million years ago) to changes in greenhouse gas concentrations, high latitude geography, and earth orbital configurations. The model shows a high sensitivity of the ocean circulation to changes in the greenhouse gas forcing, ranging from a forceful southern circulation at low CO_2 concentration (present level) to a more symmetric circulation cell with deep water formation in both hemispheres at high CO_2 concentration (8x present level). The simulated climate with 4x present level CO_2 concentration agrees generally well with climate-sensitive sediments and phytogeographic patterns. In this experiment, the model simulates strong subtropical gyres with similarities to the modern South Pacific circulation and moderate surface temperatures on the southern continent Gondwana, resulting from a strong poleward heat transport in the ocean. An even more moderate climate can be generated if high latitude land is removed so that ocean currents can penetrate into the polar regions or if orbital configurations favor high summer insolation over Gondwana.

ISSN 0397-1060

1. Introduction

The long-term climate trend during the late Paleozoic era is documented in biogeographic provinces, climate-sensitive sediments and organic productivity (e.g. coral reefs, evaporites, oil source rocks, coals, eolian sands, IRD, and glacial tillites) [*Crowley and North*, 1991; *Ziegler et al.*, 1998]. These climate proxies indicate a drastic climate transition from an Icehouse world with extensive continental ice sheets during the Carboniferous (~330 Ma) to an ice-free state in the Wordian (267 to 264 Ma). The greatest mass extinction in the Phanerozoic occurred at the Permo-Triassic boundary around 252 Ma. Several hypotheses have focused on changes in the ocean, including a possible stratified ocean with an anoxic deep sea [*Sepkoski*, 1995*; Isozaki*, 1997]. The drastic Phanerozoic-Cenozoic climate change [*Parish*, 1998] was accompanied by a large tectonic reorganization of the continents from a supercontinent Pangaea with an almost closed meridional barrier during the Permian (~290 to 252 Ma years ago) [*Seyfert and Sirkin*, 1979; *Ziegler et al.*, 1979] to the modern configuration, by a decrease of the solar insolation, and by a significant change in the Earth s orbital parameters.

Simulations with energy-balance climate models demonstrated the importance of reduced solar insolation (~3% lower than the modern value) and low atmospheric CO_2 concentration for the build-up of continental ice sheets during the Carboniferous and Early Permian [*Crowley and Baum*, 1992]. Several studies indicate that the retreat of these ice sheets during the Permian might be partially explained by an increased atmospheric CO_2 concentration from a value comparable to the modern level ~300 Ma to a quadrupled value around 265 Ma [*Crowley and Baum*, 1992; *Berner*, 1994, 1997; *Fawcett*, 1994; *Barron and Fawcett*, 1995]. Comparison of the Wordian climate derived from floral and lithological data with simulations from the GENESIS 2 climate model indicate the fit is improved if the model is forced with 4 to 8 times elevated atmospheric CO_2 level

[*Gibbs et al.*, 2001; *Rees et al.*, 2001]. Variations of the Earth s orbital parameters could also significantly change the annual range in temperature. *Gibbs et al.* [2001] showed that a combination of low CO_2 levels (such as present-day levels) and a cold summer orbital configuration produces expanded areas of permanent snow cover.

Ziegler [1998] suggested that the polar warming and a melting of the ice caps could be triggered by a northward migration of Pangaea as evidenced by a decrease of glacial tillites during the Wordian on the southern continent Gondwana. Also, he suggested that the poleward heat transport of warm polar currents might have an important effect on the warming, and this has been documented by an ocean model simulation with idealized topography [*Kutzbach et al.*, 1990]. The importance of oceanic heat transport for a large supercontinent has also been discussed in previous climate studies for Paleozoic times. For example, ocean model simulations for the geographic configuration of the Late Ordovician (~460-440 Ma) indicate an up to ~42% increase in the global ocean poleward heat transport in the southern hemisphere relative to present-day and a significant asymmetry relative to the equator [*Poussard et al.*, 1999].

The purpose of this study is to explore the role of changed radiative forcing and changes of the poleward heat transport during the Wordian. We present sensitivity experiments to investigate feedback mechanisms between various components of the climate system due to significant changes in topography and radiative forcing. In particular we are addressing the following questions: 1. How do the ocean circulation and oceanic heat transport change using a Permian land/ocean distribution and idealized bathymetry in a dynamic ocean model?, 2. How sensitive are changes of the Wordian climate and ocean circulation to changes in the atmospheric CO_2 concentration?, 3. How do changes in land configuration near the poles influence the formation of warm circumpolar currents, and how do these currents affect the continental temperatures over

Pangaea?, and 4. How well do these simulated oceanic conditions agree with the geologic evidence? For the purpose, model simulations are compared with climate-sensitive sediments [*Ziegler et al.*, 1998], with phytogeographic patterns [*Rees et al.*, 2001], and are discussed with respect to major identified data/model agreements and disagreements.

2. Model Description

2.1. The coupled model

The coupled model consists of two components, an atmospheric energy balance model and an ocean general circulation model. The use of an energy balance model for the atmosphere reduces significantly the computational costs and complexity in comparison to a fully coupled ocean-atmosphere general circulation model. The atmospheric energy balance model (EBM) has been developed by *Mikolajewicz* [1996] and has been applied to paleoclimatic studies [*Mikolajewicz*, 1996; *Mikolajewicz and Crowley*, 1997]. It assumes a balance between incoming solar short-wave radiation and outgoing long-wave radiation, which is proportional to surface temperature T_{surf}. The incoming short-wave radiation is reduced by albedo as a function of T_{surf}, by greenhouse gas absorption, and by scattering/absorption by clouds, ozone, and dust. The EBM contains a well-mixed vertical layer and is integrated for one day. The horizontal heat transport in the EBM is parameterized as advection with wind derived from an atmospheric climate model and a horizontal diffusion with a coefficient of 10^6 m^2 s^{-1}. The EBM is coupled to the ocean model via surface energy exchange and uses specified wind forcing and precipitation minus evaporation (P-E) forcing from an $4xCO_2$ companion simulation *Gibbs et al.* [2001], which used the GENESIS 2 climate model [*Thompson and Pollard*, 1995].

The heat fluxes between the EBM and ocean model are used to evaluate a new distribution of the temperature and sea ice in the mixed layer of the ocean, which is also integrated with a timestep of one day. The resulting new surface condition serves as the new lower boundary condition for the atmosphere. The atmosphere-ocean heat exchange considers a coupling coefficient of 40 Wm^{-2} K^{-1} to simulate a strong damping for small-scale temperature changes and is reduced over areas of sea ice coverage. The conductive heat flux through sea ice is inversely proportional to the ice thickness and is proportional to the difference between the air temperature and the sea surface temperature (SST) at air temperatures below freezing point.

The Hamburg large scale geostrophic ocean general circulation model (hereafter LSG) [*Maier-Reimer et al*., 1993, *Mikolajewicz and Crowley*, 1997] uses a time step of 15 days, a spatial resolution of 3.5^{o}x3.5^{o} horizontally and 22 layers vertically, and allows computationally efficient long-term model integrations of several thousand years. The model generates prognostic three-dimensional fields of the ocean currents, potential temperature, salinity, tracers, sea level, and sea ice thickness. The model includes an explicit formulation of vertical diffusion for temperature and salinity (ranging from 5 x 10^{-3} m^2 s^{-1} at the surface to 2 x 10^{-3} m^2 s^{-1} for the intermediate and deep ocean). Sea ice is advected by the mean surface velocity of the ocean and by the wind with an assumed equilibrium velocity proportional to the surface wind speed.

A simple river runoff model with a bucket depth of 30 cm is included in the ocean model. It transports the net precipitation from the land surface to the coastal ocean areas. To smooth the oceanic surface salinity field, a restoring term towards the mean with a time constant of 100 days was added to the freshwater fluxes. The model is initialized for all Wordian experiments with a mean salinity of 34.3 and a mean temperature of about 4^{o}C (world ocean s average mean temperature today). The reduction in salinity by 0.5 relative to the present-day value is based on the

assumption that water stored in the form of ice, at modern times essentially in Antarctica and Greenland, was probably not present during the Wordian.

2.2. Topography and Land-Sea Distribution

The paleogeographic basemaps including land-sea distribution, bathymetry and land surface elevation are taken from the Paleogeographic Atlas Project of the University of Chicago [*Ziegler et al*., 1997; *http://pgap.uchicago.edu*]. Continental positioning is a crucial boundary condition for the atmospheric and oceanic circulation. The ocean circulation depends on the mean depth of the ocean [*Bice*, 1997] and on the bathymetry, which is poorly known for the Middle Permian. We assume therefore a flat bottom topography with a depth of 4000 m based on the mean depth of the modern ocean. A smoothed transition from the continental shelves to the deep ocean is derived from the modern topography (Figure 1a). The deep Tethys is cut-off from the Panthalassa Ocean.

The Permian paleogeography of Pangaea is reasonably well known, except for the position of islands in the Tethys Sea which belong nowadays to Southeast Asia. *Rees et al.* [1999, 2001] discussed the uncertainties of the positions of landmasses for these regions based on climate model/data comparison. The altitude of Pangaea mountain chains has a relevant impact on the climate simulations [*Otto-Bliesner,* 1993, 1998] and has been specified for the atmospheric model simulations [*Gibbs et al.*, 2001]. The estimates of the orography are based on literature on geochronology, tectonics, sedimentary provinces, paleo-volcanism, and paleogeology. The Pangean continent in our base line experiment is extended to the pole because of the coarse resolution model grid. Sensitivity experiments explore the effect of circumpolar currents in the northern hemisphere and in the southern hemisphere (4xCO2N and 4xCO2S) when the land is removed between 70^{o}-90^{o}.

2.3. Orbital Parameters and Solar Luminosity

Previous studies [*Crowley et al.*, 1992] indicate that orbital variations could be significant on a supercontinent. To study the sensitivity of the coupled model to orbital parameters we use the same three configurations as *Gibbs et al.* [2001]: For our reference run we assume the Earth s orbit about the sun was circular (eccentricity = 0) and that the Earth s obliquity (axial tilt) was 23.5^{o}. This setting causes an equal receipt of solar insolation for both hemispheres. Two additional extreme experiments with a hot and cold summer orbit were carried out to investigate the potential impacts of the ocean circulation on surface temperatures of Gondwana and potential implications for ice-sheet reinitiation. Similar to *Crowley and Baum* [1995], we use *Berger s* [1978] extreme values for the Pleistocene with an eccentricity of 0.06 for both experiments and an obliquity of 24.5^{o} for the warm summer orbit (WSO) and 22^{o} for the cold summer orbit (CSO). The Sun s solar luminosity is thought to have been steadily increasing since formation, a consequence of conversion of hydrogen to helium. According to calculations by *Boothroyd* (see *Caldeira and Kasting* [1992]), we chose for the Middle Permian a reduction of 2.1% relative to the present-day solar constant of 1365 W m^{-2}. Decreases of the earth s rotation rate with time have been estimated from paleontological analysis [*Scrutton et al.*, 1978] and tidal analysis [*Williams et al.*, 1997]. However, changes from the Permian to present are smaller than 3% and are neglected in the atmospheric and ocean model simulations.

2.4 Atmospheric CO_2 Level

The assumption of atmospheric CO_2 level is crucial for the radiative forcing of the Earth s climate system. Here we use the functional form of greenhouse gas forcing from *Wigley* [1987] and a

coefficient from *Hansen et al.* [1988] (consistent with the IPCC 1990 report) to define the changes in the net radiative flux at the tropopause (in W m^{-2}):

$$\Delta F = 6.3 \ln(pCO_2/(pCO_2)_{ref})$$

with the preindustrial atmospheric partial pressure $(pCO_2)_{ref}$ = 280 ppmv. *Berner s* [1994] GEOCARB II geochemical model predictions suggested an increase ranging from 1x to 4x elevated CO_2 levels. We conducted four experiments with 1x, 2x, 4x, and 8x preindustrial CO_2 levels. The latter can be regarded as an upper limit and helps produce a more moderate high latitude winter as suggested by an analysis of fossil flora data [*Rees et al*., 2001].

2.5. Land Surface

A uniform vegetation (mixed tree and grassland or savanna), *Dorman and Sellers* [1989], is imposed at every land grid point and is consistent with the experiments carried out by the atmospheric model simulations [*Gibbs et al.*, 2001]. This prescribed uniformity is clearly unrealistic; for instance a significant area of central Pangaea was probably desert. However, interpretations of results in comparison with observational evidence would be even more complicated if a non-uniform vegetation is assumed because of vegetation s significant effect on climate [e.g., *Dutton and Baron* 1997, *DeConto et al*. in press]. We are planning climate model experiments for the Permian that will include prescribed vegetation based on the available data. Surface albedo over land is uniform for areas above the freezing point. Snow cover with albedo of 0.85 is assumed for areas with temperatures below the freezing point.

3. Simulation results

3.1. The Wordian 4xCO_2 baseline experiment

The Wordian 4xCO_2 experiment represents a four-times present day CO_2 concentration and will be referred to hereafter as the baseline experiment. The simulated mean global average ocean temperature for the Wordian is ~2^{o}C higher than for the modern ocean simulation (Table 1). Differences relative to the present-day climate simulations are related to, for example, increase in radiative forcing by greenhouse gases, reduction in luminosity, idealized orbital parameters, change in albedo by the reduction in sea ice distribution, and different geography and topography. The North-South gradients of sea and land surface temperatures (Figures 1b and 2a) are related to a maximal net radiative balance in the tropical region and a minimum at the poles.

The moderate high latitude marine temperatures are due to oceanic thermal inertia and warm poleward directed surface currents (Figure 3a). These water masses influence, by atmospheric advection, the annual temperatures over the continents. In the northern hemisphere, the annual temperature range is up to ~10^{o}C. In the Southern Hemisphere, the annual temperature range is up to ~40^{o}C over South Gondwana (Figure 4) with minimal temperatures of about -20^{o}C in the winter, which is about 10-15^{o}C warmer than polar climate simulated by *Gibbs et al.* [2001] (Figure 2b). The simulation produces a significant area where 2-4 months have temperatures >10^{o}C over Gondwana. As a result, the extent of the simulated polar climate biome is generally in agreement with recent Permian data-derived biome reconstructions [*Rees et al.*, 2001]. The pattern of annual salinity (Figure 1c) follows closely the prescribed P-E pattern (Figure 9d in *Gibbs et al.* [2001]). Differences in salinity of 1 unit between the southern Panthalassa and the northern hemisphere are

related to a strong poleward current (Figure 3a) in the southern hemisphere and low freshwater input along the east coast of South Gondwana.

Simulated east to west gradients of sea surface temperature in the tropical Panthalassa are about 3°C with coldest water delivered by upwelling in the east (comparable with the modern Pacific; Figure 1d). In the western Tethys Sea, sea surface temperature shows maximal values of over 30°C and low values of 27°C in lee of the equatorial island (South China) due to upwelling of subsurface water masses (Figure 1d). Strong temperature gradients (up to 20°C along the South Tethys Sea coast) are related to strong cooling of the land during winter. Low salinities in the equatorial region are a consequence of well-developed ITCZ precipitation. They are additionally influenced by the east-west mountain range near the equator [*Otto-Bliesner*, 1993, 1998] and by tropical upwelling. The general feature of the tropical ocean circulation in the eastern Panthalassa is comparable to the modern Pacific and shows significant N-S differences, in contrast to an ocean simulation with idealized symmetrical topography carried out by *Kutzbach et al.* [1990]. Typical current speeds are 5-10 cm s^{-1} in the equatorial region of the Panthalassa (Figure 3a).

Strong subtropical and polar gyres in each hemisphere, centered around 30° and 50°, are simulated for Panthalassa (Figure 1e). Their strength is comparable with the gyre in the modern subtropical South Pacific. The poleward currents in both hemispheres contribute to a warm temperate climate along the west coast of Gondwana (Figure 2a and b). On the east coast of Angara (Laurasia), a polar surface current streams southward similar to the modern Labrador Current and causes a cool climate condition around Mongolia (Figure 2b), which is in agreement with Wordian data-derived biomes [*Rees et al.*, 1999, 2001]. However, the authors suggested, on the basis of floral similarities, that the cool climate could also be explained if the position of Mongolia would be moved towards Angara.

The deep ocean, as simulated, also differs from modern. Below 1500 m depth mean salinity is 34.25 and temperature is 5.4°C (compared to 34.66 and 3.8°C for the modern ocean simulation). Main locations for deep water formation (as inferred from maps of potential energy loss by convection; Figure 1f) are northeastern Panthalassa in the northern winter and southeastern Panthalassa in the southern winter. The deep circulation in high latitudes is opposite to the surface circulation (Figure 3b). A powerful westward flow moves across Panthalassa near 70°. At the east coast of Pangaea, deep western boundary currents circulate in both hemispheres towards the equator. This feature is in agreement with the idealized model of *Stommel and Arons* [1960]. They envisioned the ocean as a two-layer model with localized sinking at both hemispheres from the upper to the lower layer, and a wide spread of water masses from the abyssal layer into the wind driven upper layer. In accordance with their theory, low current velocities with minima around 30° are simulated in the interior of Panthalassa, which might have implications for an accumulation of organic material from the surface. Remineralisation and oxidation of the accumulated organic matter might cause anoxic conditions in these locations.

3.2. Response of the simulated Wordian climate to changes in atmospheric CO_2

An increase in atmospheric CO_2 concentration from a value comparable to the modern level around 300 Ma to a quadrupled value around 250 Ma has been suggested by geochemical model calculations [*Berner,* 1994*; Berner,* 1997]. To investigate the sensitivity of the ocean heat transport and deep sea ocean circulation with increasing atmospheric CO_2, three additional experiments were carried out with 1x, 2x, and 8x elevated CO_2 levels and corresponding changes in the radiative forcing of 0, 4.3, and 13.1 W m^{-2}. Differences in global average of sea surfaces temperatures between the 8xCO_2 level and 1xCO_2 are 7.1°C (Table 1) and more than 8°C in the Tethys Sea

(Figures 5a and c). The $1xCO_2$ simulation fails to generate moderate climate in southern Gondwana as a result of the cool surface temperatures, and hence is at odds with reconstructed biomes [*Rees et al.,* 2001], while the $8xCO_2$ simulation produces the most moderate climate (Figure 5c). However, the $8xCO_2$ simulation produces a very warm mid-latitude climate (20^oC isoline at a latitude of ~40^o) and high latitude climate, which are in conflict with BIOME reconstruction from *Rees et al.* [2001]. Pole to equator gradients of air surface temperature in the $1xCO_2$ experiment (Figure 5b) are estimated to be ~10^oC higher than the $4xCO_2$ baseline experiment because of effective sea-ice albedo feedback in the northern hemisphere. The model simulations indicate a sensitive response of the change in sea-ice extent in the northern hemisphere to an increase of radiative greenhouse gas forcing (Figure 6a and b). Sea-ice coverage in the northern hemisphere in the $1xCO_2$ experiment would be at odds with water masses derived from the climate-sensitive sediments (see section 5). The area covered by sea-ice is decreased by ~1/3 if the atmospheric CO_2 concentration is doubled from the 1 to $2xCO_2$ (Figure 6b, Table 1).

Using the zonal average profile of net radiation for annual mean conditions at the top of the atmosphere (Q_{TA}), we can estimate the total poleward heat transport in the ocean—atmosphere system (T_{TOT}) as a sum of the poleward heat transport by the atmosphere (T_A) and by the ocean (T_{OC}):

$$\begin{aligned} Q_{TA} &= \int_{top} (1 - A)\, Q_{SW} - Q_{LW} dt \approx 0 \\ T_A + T_{OC} &= -\int_{\phi'=\phi}^{\pi/2} Q_{TA}\, 2\pi R^2 \cos\phi'\, d\phi' \end{aligned} \qquad (2)$$

where Q_{SW} and Q_{LW} are short-wave and long-wave radiation, A is albedo and R is earth radius.

The global annual mean and zonally averaged heat transport for the $4xCO_2$ experiment is displayed in Figure 7a. The global heat transport has some similarities to the modern one (not shown here) and is in agreement with other Phanerozoic climate studies [*Poussart et al.*, 1999]. The transport is

generally dominated by the atmosphere, but in southern low latitudes by the ocean. The oceanic heat transport for the present-day (Figure 7b) is comparable with previous simulations of *Maier-Reimer et al.* [1993], which is at the lower bounds of observations as a result of the coarse model resolution. Our simulations produce considerably larger heat transport for the mid and high latitudes (up to 1 PW at 50^{o}S) than found in the study of *Gibbs et al*. [2001] where the ocean heat transport estimate is based on a heat diffusion parameterization. Our results are more in agreement with earlier results of *Kutzbach and Ziegler* [1993] who used a prescribed heat transport from an ocean simulation with idealized symmetric topography [*Kutzbach et al.*, 1990]. The oceanic heat transport changes significantly for the Wordian simulations especially in the northern hemisphere, as the CO_2 level changes. For 1xCO_2, large sea ice coverage in the northern hemisphere prevents deep-water formation in the northern high latitudes resulting in a thermohaline circulation dominated by a southern circulation cell (Figure 8a). Experiments with increased CO_2 levels and decreased sea ice coverage indicate formation of deep water in the northern high latitudes and a generation of a northern circulation cell (Figure 8c-d). Even with higher CO_2 levels the southern circulation cell is stronger as a consequence of the asymmetrical land-sea distribution (a symmetrical cell can be obtained if symmetrical continent configuration and surface buoyancy forcing is applied [*Kutzbach et al*., 1990]).

3.3. Response to circumpolar currents

Ziegler [1998] suggested that the absence of warm polar currents, as occurs for example in experiments without a 3-D OGCM, might explain the high-latitude cold bias of recent Permian climate studies as inferred from data/model comparisons [*Rees et al*., 2001]. To explore this possibility in greater detail, experiments 4xCO_2N and 4xCO_2S use the same boundary conditions as

the Wordian baseline experiment but include the possibility of a northern and a southern circumpolar current by removing land between 70^{o} to 90^{o}. Global averages do not change dramatically in these runs, but the resulting changes of currents have an impact on the climate conditions over high latitude land masses (Figure 9). With a circumpolar current, polar air surface temperatures are above the freezing point in the annual averages (Figure 9a and c). Note that the boundary conditions used (section 2.2) exaggerated the amount of polar land. In reality, these sensitivity experiments provide climate conditions that might have prevailed.

In experiment $4xCO_2N$, the warm eastward moving currents of middle north latitudes bend to the north (comparable with the flow of the present North Atlantic current into the Arctic Region) and joins the northern circumpolar current (Figure 9b). A similar feature is simulated with a southern circumpolar current (Figure 9d). Differences between these simulations are related to the asymmetrical continent configuration and the imposed wind stress (which is for all experiments to be the same). The poleward heat transport into the circumpolar currents generates a warmer climate along the adjacent coasts over both Angara and Gondwana respectively. Air surface temperatures in the southern polar region are comparable with those on the modern Norwegian Coast (e.g. near Bod) influenced by the North Atlantic Current and are up to 8^{o} C warmer than the simulated air surface temperatures in the Wordian baseline simulation (section 3.1).

3.4. Response to changes of the orbital parameters

Two extreme orbital configurations, one with hot summer orbit (HSO) and one with cold summer orbit (CSO) are considered. Otherwise, the same boundary conditions as for the Wordian baseline experiment with circular summer orbit (section 3.1) are applied. High-latitude summer temperatures are sensitive to changes in the orbital configuration and play a critical role in snow

accumulation and formation of continental ice sheets in these areas. Early Jurassic EBM simulations result in maximum surface temperature changes of up to ~15 ^{o}C [*Crowley et al.*, 1992]. Simulations of *Gibbs et al.* [2001] indicate that significant differences between HSO and CSO configurations result in some changes in south polar snow accumulation and hence affect high-latitude climate reconstructions. Here, orbital configurations are selected such that the southern hemisphere summer will be warmest with HSO and northern hemisphere will be warmest with CSO. Our simulations show HSO minus CSO differences in summer surface temperatures for the southern hemisphere (Figure 10a) of ~+20 ^{o}C centered over Gondwana and for the northern hemisphere of ~-10 ^{o}C centered over Euramerica (Figure 10b). These significant temperature changes have implications for the length of the growing season and calculation of modeled biome in a fully coupled ocean-atmosphere climate model. The positive temperature anomaly in the northern hemisphere in Figure 10a may be due to a positive ice albedo feedback mechanism in the WSO experiment. Changes of the orbital parameters have only little effect on the global annual mean air surface and ocean temperatures (Table 1), similar to results from the Late Ordovician climate sensitivity experiments of *Poussart et al.* [1999].

5. Comparison with Climate-Sensitive Sediments

Ziegler et al. [1998] constructed climate maps for the Wordian (Figure 11a) based upon Wordian sediments and their present-day relationship of sediments to characteristic water masses (Table 2). The climate-sensitive sediments have been compared with modern marine climate properties, in particular temperature, salinity and productivity related effects. The water mass boundaries listed in Table 2 are based on a summary of parameters derived from ocean scale atlases. The boundaries of characteristic water masses (defined by specific temperature and salinity ranges and strength in

upwelling) are chosen somewhat arbitrarily because it is difficult to select particular values that universally represent significant climate changes and transitions on the Paleozoic time scale. The water masses of *Ziegler et al.* [1998] are classified in eight categories (Table 2). These are briefly described (Figure 11a) and then compared with our model simulations for the Wordian (Figure 11b):

1. Glacial climate:

Data: Occurrence of permanent ice flows (like most of the modern Arctic Ocean, or ice shelf of Antarctica) generated by outflow of cold air. Tills could be expected along mountainous coasts of these regions. Sediments of this category are known in the Early Permian but have not been found in Wordian rocks.

Model: Glacial climates (sea surface temperatures < -1.8°C) are not simulated by the 4xCO_2 Wordian baseline experiment.

2. Cold temperate climate:

Data: The water masses are defined by the extent of sea ice in the winter season and correspond closely to the 0°C isotherm (e.g. similar to conditions in the modern Labrador Current). Dropstones and rhythmites would be indicative of this environment in the fossil record and have been identified in the geological record of Tasmania along the southeastern coast of Gondwana (Figure 11a).

Model: The model (Figure 11b) simulates moderate conditions along the south-polar east coast from Gondwana where data indicate a cold temperate condition. Warm conditions (sea surface temperatures of ~4°C in winter times; Figure 4c) are related to the heat transport by polarward currents modeled for these regions. In an effort to resolve this data/model discrepancy we propose

that the Tasmanian seas might represent a re-entrant in the coast, isolated from the warming effects of the open ocean currents.

3. Wet temperate climate:

Data: Temperatures between 0°C and 20°C and brackish conditions (salinity below 32) define this climate zone (for example modern Baltic Sea or Canadian West Coast). Peats are characteristically developed around the margins of these characteristic water masses and organic muds are commonly associated in the center of these areas with high precipitation. The swamp deposits depend on consistency of rainfall through the annual cycle, or at least through the warmer months (Lottes and Ziegler, 1994), and for confined seaways or broad shallow shelves this translates into lowered salinities. The associated surface runoff provides for abundant nutrients and a stratified water column which in turn allows for organic preservation. The geological data (Figure 11a) for this water mass are best seen around Angara but also occur around southern Gondwana.

Model: Simulated high precipitation [*Gibbs et al.*, 2001] and low salinities (Figure 1b) of the high-latitude west coasts of Angara agree with the geological recognition of the wet temperate climate category. In addition, model results show wet temperate regions in northern India along the shore of the southern Tethys Sea similar to the geological findings. These climate conditions are essentially related to the advection of moist tropical air masses and enhanced precipitation. Interestingly, the model shows a wider extent of this water mass type than had been inferred from the geological data but the model results are nevertheless entirely consistent with the data. Here the original water mass interpretation was simply too conservative.

4. Temperate climate:

Data: Temperature in this climate zone ranges 0^{o}C and 20^{o}C and salinity between 32 and 37 (e.g. Kuroshio Current for modern climate). No particular climate indicators have been identified for this zone, but peats are quite common due to low evaporation rates in mid to high latitudes.

Model: The equatorial margin of the water mass in this climate zone is placed around 30^{o} latitude for the Wordian $4xCO_2$ simulation (Figure 11b), similar to the reconstructed equatorial margin from climate-sensitive sediments (Figure 11a). The bias between model results and the reconstructions on the West Coast of Pangaea can be explained by the more poleward location of main upwelling areas, which are centered in the model around the equator as a response to the wind stress and topography.

5. Cool subtropical upwelling zones:

Data: This category is defined by zones, which are mainly limited to the subtropical belt and equatorial region where Ekman-induced upwelling produces high organic productivity and nutrient content. Formation of organic muds and phosphorites constitutes the recognition of these upwelling zones. No attempt was made to map the equatorial upwelling zone as the Permian ocean floor has been subducted and the sedimentary evidence destroyed.

Model: Upwelling is mapped as green shaded areas and is defined to have upward current velocities greater than 1×10^{-6} m s^{-1} (Figure 11b). Typical regions are the coastal upwelling along the west coast of Gondwana at locations comparable with modern Californian coast or the Coast of Peru. A strong upwelling belt is located along the Equator similar to the modern Pacific and around islands. This equatorial upwelling includes shallow platform seas of the South China microcontinent and is actually supported by the presence of organic rich shales and phosphorites.

These were originally interpreted as indicating the wet tropical water mass (Figure 11a) but the upwelling intrepretation fits equally well.

6. Dry subtropical climate:

Data: Areas with low precipitation minus evaporation with salinity greater than 37 provide favorable conditions for evaporite deposition in coastal lagoons and broad platform seaways (Figure 11a).

Model: Low precipitation and high salinities are simulated along the southeastern Tethys Sea (Figure 1c), South China, or the West Coast of Euramerica in agreement with the geological evidence. In addition, embayments along the northern coast of Euramerica have been identified to be dry from model simulations (Gibbs et al. in press) and geological data. However, the ocean model does not resolve this area because of the coarse resolution of the model (Figure 11b).

7. Tropical climate:

Data: Surface temperatures greater than 20 ^{o}C and normal salinity, which allows carbonate build-up and bottom productivity, charaterize this water mass (Figure 11a). Carbonate build-ups are generally not found in the geological past above 35^{o} of latitude, as shown by paleomagnetic data [*Hulver et al.*, 1997]. This latitudinal restriction constitutes the zone of light penetration to the sea floor as controlled by the Sun's zenith angle (Ziegler et al., 1984).

Model: Model simulations (Figure 11b) are in agreement with climatic reconstructions (Figure 11a), but deviations on the west coast of Pangaea are associated with upwelling areas, which cannot be entirely resolved with the coarse model resolution.

8. Wet Tropical:

Data: Areas with tropical temperatures and salinities below 32 are defined to have relatively brackish conditions. Organic-rich shales do not seem to be associated with wet tropical climate at

modern times, but they almost certainly occurred in the Wordian (e.g. in the South China, Figure 11a).

Model: Wet tropical conditions are simulated in the southern Tethys Sea, for the east coast of North China, and the southern coast of South China (Figure 11b). Such areas are characterized by high river runoff, and/or high precipitation (e.g. along the intertropical convergence zone) and correlate well with tropical coals of these areas.

6. Summary and Discussion

We simulated the Wordian climate with a coupled atmosphere-ocean model (EBM and LSG) using realistic land ocean geometry. The model results ($4xCO_2$ baseline experiment) produce (1) surface water masses with temperature characteristics which are warmer and fresher than at modern times in the high latitudes, (2) a strong westward equatorial current which is blocked by islands at the eastern Tethys Sea, (3) warm poleward currents along the Tethys coast and east coast of Gondwana, (4) cold equatorward currents along the east coast of Angara, (5) two large meridional circulation cells with deep water formation at the poles, and (6) a warm deep sea with low current speed in the eastern equatorial Panthalassa. The model results were compared with climate-sensitive sediments (section 5) and with other climate simulations. The $4xCO_2$ baseline experiment shows the best agreements with the paleoclimatic data (section 5). Our experiments suggest that a low CO_2 concentration ($1xCO_2$) would cause significant data-model disagreements. Low CO_2 concentrations would be favorable to explain the glacial climate over Gondwana during the Permo-Carboniferous glaciation [*Crowley and North*, 1981], whereas using high CO_2 ($8xCO_2$ experiment) concentration simulates too warm conditions in the high latitudes and would be in conflict to CO2 estimates from *Berner* [1997]. Uncertainties remain, for example related to an inadequate

representation of the water-vapor feedback mechanism in energy balance models [*Pierrehumbert*, 1995; *Bates,* 1999], which might alter our results as well as those from previous studies significantly. Also, consideration of Permian to modern changes in the aerosol loading by e.g. volcanic activities related to mid-ocean ridges or subduction processes and concentration of trace gases might be relevant for the radiative budget, but there are no estimates of these properties available so far. We also infer from our simulations that changes of the astronomical parameters have a significant impact on the climate over Gondwana, a general agreement with previous studies [*Crowley et al.*, 1992]. The solutions of the simulations with the coupled atmospheric energy balance ocean general circulation model might result in multiple steady states. However, we expect that the stability of our simulations is robust because of the asymmetry of the geography of Pangea in respect to the equator. Preliminary results from simulations with a transient CO_2 radiative forcing from two times CO2 to one times CO2 support these findings.

Interestingly, we showed that an existence of circumpolar currents would influence the temperature of adjacent high latitude coasts. In comparison with the previous study of *Gibbs et al.* [2001], temperature changes over Gondwana were simulated to be up to 15^{o}C higher in the annual mean. Paleogeographic and topographic reconstruction of islands is still very speculative. For example, we deduce from our experiments and comparison with those of *Kutzbach* et al. [1990] that a more southward position of South China would imply a higher heat transport into the Tethys Sea and a warming of the adjacent coasts.

7. Conclusion

The results of our simulations emphasize that ocean poleward heat transport is important for climate simulations. Previous model studies using parameterized simplified ocean heat transport

identified a significant model-data disagreement by estimating a too cold polar climate over Gondwana. In contrast, our simulations with the energy balance climate model coupled to a dynamic ocean model show considered warming in the polar regions. A four times elevated CO_2 level would generally match the reconstructions from climate-sensitive sediments and phytogeographic patterns. Regions of slow currents in the deep Panthalassa have implications for carbon accumulation and low oxygen conditions. The simulated Panthalassa deep sea circulation shows a high sensitivity to the ice-albedo feedback and radiative greenhouse gas forcing.

The outcome of this study will be helpful for the design of future asynchronous or fully coupled ocean-atmosphere general circulation studies, which could include sensitivity experiments in respect to water-vapor formulations and dust/aerosol estimates, as well as changes in the geography and ocean topography. We have started to carry out such simulations with an idealized geography. In addition, a coupling of ocean-atmosphere climate models to the biogeochemical models would give a more detailed insight for possible anoxic conditions in the Panthalassa ocean and might have implications for the Late Permian mass extinction.

Acknowledgements. We thank Cornelia Winguth for reading this manuscript, David Archer for fruitful discussions and Pat Behling for providing the forcing fields from the GENESIS run of *Gibbs et al.* [2001]. This work was done in collaboration with the Max-Planck-Institut fuer Meteorology, the Deutsche Forschungsgemeinschaft SPP 1054, and with the University of Chicago (supported by the Packard Foundation). John Kutzbach is supported by NSF grant ATM-9815980.

References

Bates, J.R. A dynamical stabilizer in the climate system: a mechanism suggested by a simple model, *Tellus*, 51A, 349-372, 1999.

Barron, E. J., and P. J. Fawcett, The climate of Pangaea: A review of climate model simulations of the Permian, in *The permian of Northern Pangaea: Volume 1: Paleogeography, Paleoclimates, Stratigraphy*, edited by P. A. Scholle, T. M. Peryt, and D. S. Ulmer-Scholle, pp.37-52, Springer-Verlag, New York, 1995.

Berger, A. L., Long-term variation of calcoric insolation resulting from the Earth s orbital elements, *Quat. Res.*, 9, 139-167, 1978.

Berner, R. A., GEOCARBII: A revised model of atmospheric CO_2 over Phanerozoic time, *Am. J. Sci.*, 294, 56-91, 1994.

Berner, R. A., The rise of plants and their effect on weathering and atmospheric CO2, *Science*, 276, 544-546, 1997.

Bice, K., An investigation of early Eocene deep water warmth using uncoupled atmosphere and ocean general circulation models: Model sensitivity to geography, initial temperatures, atmospheric forcing and continental runoff, *Ph.D. thesis*, University Park, Pennsylvania State University, 363p., 1997.

Caldeira, K., and J. F. Kasting, The life span of the biosphere revised, *Nature*, 360, 721-723, 1992.

Crowley, T. J., and S. K. Baum, Modeling late Paleozoic glaciation, *Geology*, 20, 507-510, 1992.

Crowley, T. J., and S. K. Baum, Reconciling Late Ordovician (440 Ma) glaciation with very high (14x) CO_2 levels, *J. Geophys. Res., 100*, 1093-1101, 1995.

Crowley, T. J., and G. R. North (eds.), *Paleoclimatology*, Oxford University Press, 339 pp., 1991.

Crowley, T. J., S. K. Baum, and W. T. Hyde, Milankovitch fluctuations on supercontinents, *Geophys. Res. Let.*, 19, 793-796, 1992.

DeConto, R. M., W. W. Hay, S. L. Thompson, and J. Bergengren, Late Cretaceous climate and vegetation interaction: The cold continental interior paradox, in *Evolution of Cretaceaous Oceans/Climate Systems*, edited by E. Barrera and C. Johnson, Evolution of Cretaceous Oceans/climate Systems, in press.

Dorman and Sellers, A global climatology of albedo, roughness lenght and stomatal resistance for atmospheric general models as represented by the simple biosphere model (SiB), *J. Appl. Meteor.*, 28, 833-855, 1989.

Dutton, J. F., and E. J. Barron, Miocene to present vegetation changes, a possible piece of the cenozoic puzzle, *Geology*, 25, 39-41, 1997.

Fawcett, P. J., Simulation of climate-sedimentary evolution: A comparison of climate model results with the geologic record for India and Australia, PhD Thesis, University Park, Penn State University, 327 p., 1994.

Gibbs, M. T., P. M. Rees, J. E. Kutzbach, A. M. Ziegler, P. J. Behling, and D. B. Rowley, Simulation of Permian climate and comparison with climate-sensitive sediments, *J. Geology*, in press, 2001.

Hansen, J., I. Fung, A. Lacis, D. Rind, S. Lebedeff, R. Ruedy and G. Russel, Global climate changes as forecast by the GISS s three-dimensional model, *J. Geophys. Res.*, 93, 9341-9364, 1988.

Hulver, M. L., A. M. Ziegler, D. R. Rowley, and M. T. Gibbs, Global latitudinal distribution of Permian to Recent climate-sensitive sediments, *Geological Society of America Abstracts with Programs*, 29, 6, 1997.

Isozaki, Y., Permo-Triassic boundary superanoxia and stratified superocean: Records from lost deep sea, *Science*, 276, 235-238, 1997.

Kutzbach, J. E., P. J. Guetter, and W. M. Washington, Simulated circulation of an idealized ocean for Pangaean time, *Paleoceanography*, 5, 299-317, 1990.

Kutzbach, J.E., and A.M. Ziegler, Simulation of Late Permian climate and biomes with an atmosphere/ocean model: comparisons with observations, in: *Palaeoclimates and Their Modelling with Special Reference to the Mesozoic Era*. Philosophical Transactions of the Royal Society of London, Ser. B, 341, pp. 327-340, 1993.

Lottes, A.L., and A.M. Ziegler, World peat distribution and the seasonality of climate and vegetation, *Palaeogeography, Palaeoclimatology, Palaeoecology,* 106, 23-37, 1994.

Maier-Reimer, E., U. Mikolajewicz, and K. Hasselmann, Mean circulation of the Hamburg LSG OGCM and its sensitivity to the thermohaline surface forcing, *J. Phys. Oceanogr.*, 23, 731-757, 1993.

Mikolajewicz, U., A meltwater induced collapse of the "conveyor belt" thermohaline circulation and its influence on the distribution of $\Delta^{14}C$ and $\delta^{18}O$ in the oceans, Rep. 189, Max-Planck-Inst. fuer Meteorol., Hamburg, Germany, 1996.

Mikolajewicz, U., and T. J. Crowley, Response of a coupled ocean/energy balance model to restricted flow through the central american isthmus, Paleoceanography, 12, 429-441, 1997.

Otto-Bliesner, B. L., Tropical mountains and coal formation: A climate model study of the Westphalian (306 Ma), *Geophys. Res. Let.*, 20, 1947-1950, 1993.

Otto-Bliesner, B. L., Effects of tropical mountain elevations on the climate of the Late Carboniferous: Climate model simulations, in *Tectonic Boundary Conditions for Climate Reconstructions*, edited by T. J. Crowley and K.C. Burke, pp. 100—115, New York, Oxford University Press, 1998.

Parish, J.T. (ed), *Pre-Quaternary climate from the geologic record*, Columbia University Press, New York, 338pp., 1998.

Pierrehumbert, R.T., Thermostats, radiator fins, and the local runaway Greenhouse, *J. Atmos. Sci*., 52, 10, 1784-1806, 1995.

Poussard, P. F., A. J. Weaver, and C. R. Barnes, Late Ordovician glaciation under high atmospheric CO2: A coupled model analysis, *Paleoceanography*, 14, 542-558, 1999.

Rees, P. M., M. T. Gibbs, A. M. Ziegler, J. E. Kutzbach, and P J. Behling, Permian climates: evaluating model predictions using global paleobotanical data, *Geology*, 27, 891-894, 1999.

Rees, P. M., A. M. Ziegler, M. T. Gibbs, J. E. Kutzbach, P. J. Behling, and D. B. Rowley, Permian phytogeographic patterns and climate data-model comparisons, *J. Geology*, in press.

Scrutton, C. T., Periodic growth features in fossil organisms and the length of the day and the month, in *Tidal Friction and the* Earth rotation, edited by P. Brosche and J. Suendermann, pp. 154-196, Springer-Verlag, New York, 1978.

Seyfert, C. K., and L. A. Sirkin, Earth history and plate tectonics, Harper and Row, 2nd edition, New York, p. 600, 1979.

Sepkoski Jr, J. Patterns of Phanerozoic extinction: A perspective from global data bases, in *Global Events and Event Stratigraphy in the Phanerozoic,* edited by O.H. Walliser, pp. 36-51, Springer Verlag New-York, 1995.

Stommel, H., and A. B. Arons, On the abyssal circulation of the World Ocean, II, An idealized model of the circulation pattern and amplitude in oceanic basins, *Deep Sea Res*., 6, 217-233, 1960.

Thompson, S.L., and D. Pollard, A global climate model (GENESIS) with a land-surface transfer scheme (LSX). Part I: Present-day climate, *J. Climate*, 8, 736-761, 1995.

Wigley, T. M. L, Possible climate change due to SO2-derived cloud condensation nuclei, *Nature*, 339, 365-367, 1989.

Williams, D. M., J. Harkin, and A.H. N. Rice, Umbers, ocean crust and the Irish Caledonides: Terrane transpression and the morphology of the Laurentian margin, *J. Geol. Soc. London*, 154, 829-838, 1997.

Ziegler, A.M., Warm polar currents, *EOS Trans. 78*, Spring Meeting Supplement, 1998.

Ziegler, A.M., Hulver, M.L., and D.B. Rowley, Permian World Topography and Climate, in *Late Glacial and Postglacial Environmental Changes-Quaternary,* edited by I.P. Martini, pp. 111-146, Oxford University Press, New York, 1997.

Ziegler, A. M., C. R. Scotese, W. S. McKerrow, M. E. Johnson, and R. K. Bambach, Paleozoic paleogeography, *Annual Reviews of Earth and Planetary Sciences*, 7, 743-502, 1979.

Ziegler, A.M., M.L. Hulver, A.L. Lottes, and W.F. Schmactenberg, Uniformitarianism and palaeoclimates: Inferences from the distribution of carbonate rocks, in *Fossils and Climate,* edited by P.J. Brenchley, ed., pp. 3-25, John Wiley & Sons Ltd., Chichester, 1984.

Ziegler, A. M., M.T. Gibbs, and M.L. Hulver, A mini-atlas of oceanic water masses in the permian period, *Procceedings of the Royal Society of Australia*, 110(1/2), 323-343, 1998.

Figure captions

Table 1. Climate simulations for the Wordian ocean are compared with the present-day experiment (preindustrial CO_2 concentration of 280 ppm). The Wordian experiments in response to 4 times peindustrial CO_2 concentration ($4xCO_2$) are defined to be the baseline experiment. Additional experiments investigate the change of the Wordian climate due to changes in the radiative greenhouse gas forcing ($1xCO_2$, $2xCO_2$, and $4xCO_2$). Experiments $4xCO_2$ with northern circumpolar current (N) and southern circumpolar current (S) between 70^o-90^o explore the effect of warm polar currents on the Permian climate in high latitudes. The response of the Wordian climate to different orbital configurations (cold summer orbit CSO and hot summer orbit HSO) is studied by using experiments $4xCO_2$CSO and $4xCO_2$HSO. Annual averages are given for global mean temperature of the ocean T_o, mean sea surface temperature (SST), mean surface air temperature (SAT), and poleward heat transport of the ocean (T_{oc}) at 30^oN and 30^oS. A_{ICE} denotes the ratio of ice-covered area to total surface ocean area for the North Hemisphere (NH) and South Hemisphere (SH). V_{ICE} is the total ice volume in percent.

Table 2. Surface water mass classification.

Figure 1. Model topography (a) and annual-average of modeled sea surface temperature (b), surface salinity (c), vertical velocity between surface layer and second model layer (d), barotropic stream function (e), and potential energy loss by convection (f) for the Wordian climate with $4xCO_2$ (contour interval: 0.5km, 2^oC, 0.5, 1.5 10^{-6} m s^{-1}, and 10^6 m^3 s^{-1}).

Figure 2. Annual-average of air surface temperature in ^{o}C for the Wordian climate with $4xCO_2$ (a) and differences of (a) to the study of *Gibbs et al.* [2001] (b) (contour interval: 10^{o}C and 1^{o}C).

Figure 3. Annual-average of horizontal velocity at the surface (a) and in the deep sea (~3200 m; b) for the Wordian climate with $4xCO_2$.

Figure 4. Left: January (a) and July (c) modeled sea surface temperature for the Wordian climate with $4xCO_2$ (contour interval: 2^{o}C). Right: January (b) and July (d) air surface temperature for the $4xCO_2$ experiment (contour interval: 5^{o}C).

Figure 5. Left: Annual-average of modeled sea surface temperature for the Wordian climate with $1xCO_2$ (a), and $8xCO_2$ (c) (Contour interval: 2^{o}C). Right: Annual-average of air surface temperature in ^{o}C for the $1xCO_2$ (b) and $8xCO_2$ (d) experiment (contour interval: 5^{o}C).

Figure 6. Annual-average of sea ice distribution in [m] for the $1xCO_2$ (a) and $2xCO_2$ (b) Experiment (contour interval: 0.1 m).

Figure 7. Meridional profile of the poleward transport of heat in PW (10^{15} W). (a) Heat transport by the ocean (T_{OC}), atmosphere (T_A) and total heat transport ($T_{TOT} = T_A + T_{OC}$) for the Wordian climate with $4xCO_2$. (b) Heat transport by the ocean (T_{OC}) for the $1xCO_2$, $2xCO_2$, $4xCO_2$, $8xCO_2$, and present-day experiment. For comparison, heat transport calculated by diffusive parameterization in the mixed-layer for the Wordian with $4xCO_2$ [*Gibbs et al.*, 2001] is displayed.

Figure 8. Zonally averaged Atlantic meridional circulation for the Wordian climate with 1xCO_2 (a), 2xCO_2 (b), 4xCO_2 (c), and 8xCO_2 (d) (contour interval: 5 Sv = 5 x 10^6 m^3 s^{-1}).

Figure 9. Left: Annual-average of modeled difference in air surface temperature in ^oC between the 4xCO_2 experiment with northern circumpolar current (a) and southern circumpolar current (b) and the 4xCO2 baseline experiment. (Contour interval: 5^oC). Right: Annual-average surface velocities for the 4xCO_2 experiment with northern circumpolar current (a) and southern circumpolar current (b).

Figure 10. Difference of air surface temperature in January (a) and July (b) between the simulation with hot summer orbit (4xCO_2HSO) and cold summer orbit (4xCO_2CSO) configuration. Note that the cold summer orbit configuration for the southern hemisphere corresponds to a hot summer orbit configuration for the northern hemisphere (contour interval: 2^oC).

Figure 11. (a) Wordian (Kazanian, Early Maokouan) climate sensitive sediments and reconstructed water masses from *Ziegler et al.* [1998]. (b) Water mass classification derived from the climate simulation with 4xCO_2.

Table 1. Results from the Wordian ocean simulations (annual averages):

Experiments	T_o [°C]	SST[°C]	SAT [°C]	$A_{ice(NH)}$ [%]	$A_{ice(SH)}$ [%]	V_{ice} [10^{12} m^3]	T_{oc} [PW] at 30°S	T_{oc} [PW] at 30°N
Present Day	5.0	19.5	12.5	8.5	3.8	6.4	-1.45	1.38
Control (4xCO_2)	7.0	21.0	15.3	0.0	0.0	0.0	-1.71	1.05
1xCO_2	4.5	16.0	9.5	12.4	0.3	0.9	-2.40	0.15
2xCO_2	5.6	18.8	12.9	2.5	0.1	0.1	-1.65	1.08
8xCO_2	8.5	23.1	17.5	0.0	0.0	0.0	-1.78	1.14
4xCO_2N	6.7	20.7	15.2	0.0	0.0	0.0	-1.90	0.89
4xCO_2S	6.4	20.7	15.7	0.0	0.0	0.0	-1.74	1.06
4xCO_2CSO	6.9	21.1	15.3	0.2	0.0	0.0	-1.84	1.02
4xCO_2HSO	7.3	21.2	15.5	0.0	0.0	0.0	-1.74	1.05

Table 2. Surface water mass classification.

Climate Zone	Water mass essentials	Geological recognition
Glacial	Surface permanently frozen SST <-1.8 °C	Marine till
Cold Temperate	Winter ice flows SST —1.8-0℃	Dropstones, rhythmites
Wet Temperate	Brackish surface water SST 0-20 °C, salinity <32	Temperate peats, organic rich shales
Temperate	Mixed water column SST 0-20 °C, salinity 32-37	Clastics
Cool Subtropical	Upwelling currents Vertical velocity w > 1 x 10^{-6} m s^{-1}	Organic-rich shales, phosphorites, cherts
Dry Subtropical	High evaporation Salinity >37	Gypsum, halite, sabkha facies
Tropical	Deep light penetration SST >20 °C, salinity 32-37	Carbonates, oolites, coralgal reefs
Wet Tropical	High precipitation or continental runoff SST >20 °C, salinity < 32	Tropical peats, muddy sediments

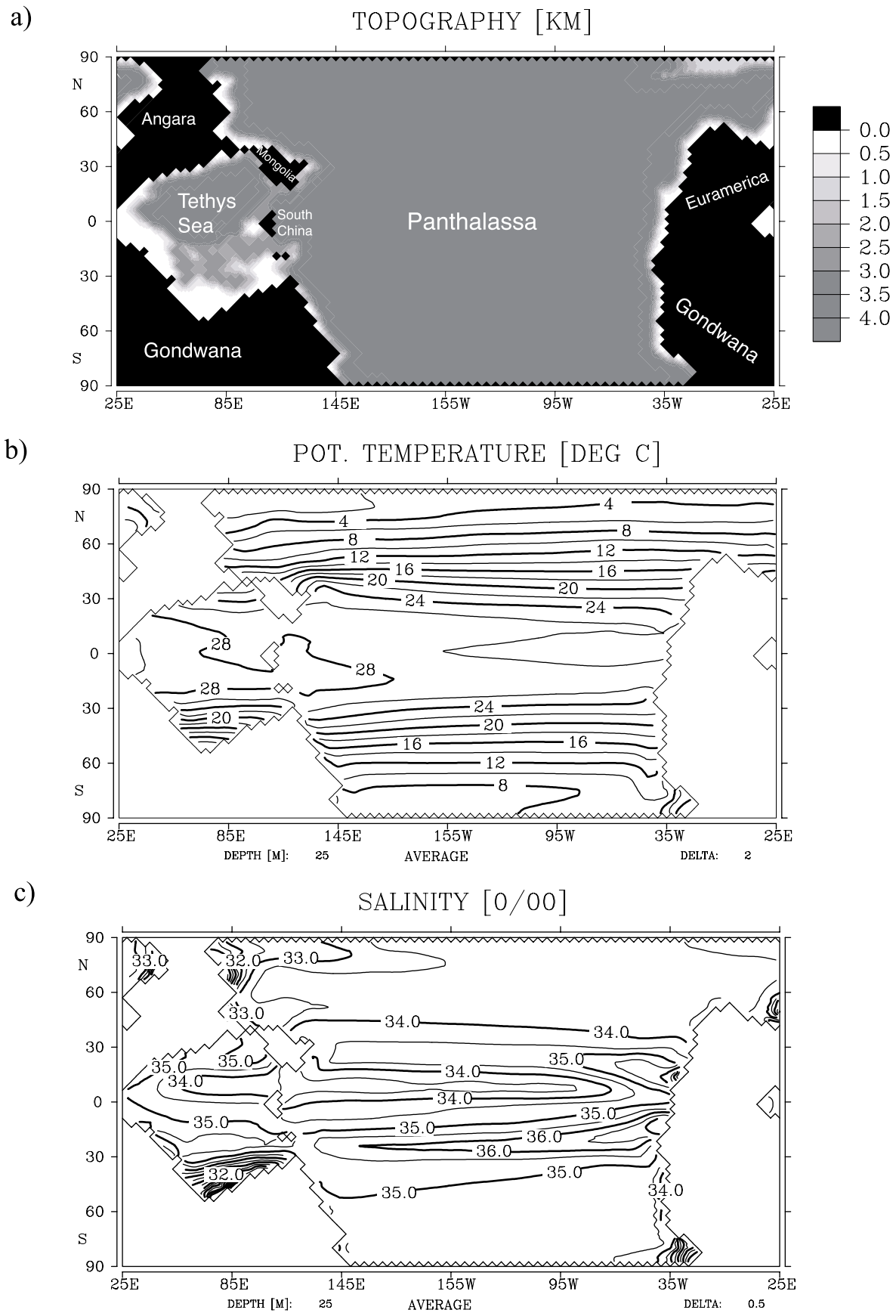
a)
TOPOGRAPHY [KM]
Angara
Mongolia
Tethys Sea
South China
Panthalassa
Euramerica
Gondwana
Gondwana
0.0
0.5
1.0
1.5
2.0
2.5
3.0
3.5
4.0
b)
POT. TEMPERATURE [DEG C]
DEPTH [M]: 25
AVERAGE
DELTA: 2
c)
SALINITY [0/00]
DEPTH [M]: 25
AVERAGE
DELTA: 0.5
90 N 60 30 0 30 60 S 90
25E 85E 145E 155W 95W 35W 25E

FIGURE 1

d)

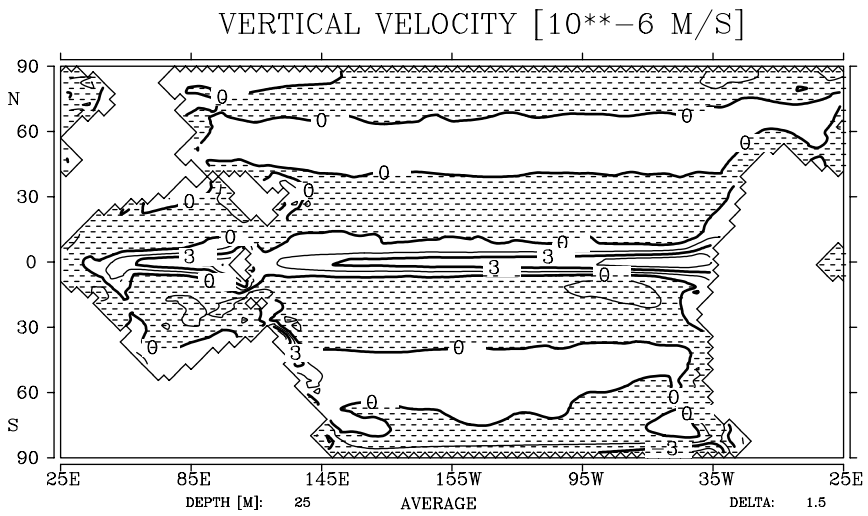

e)

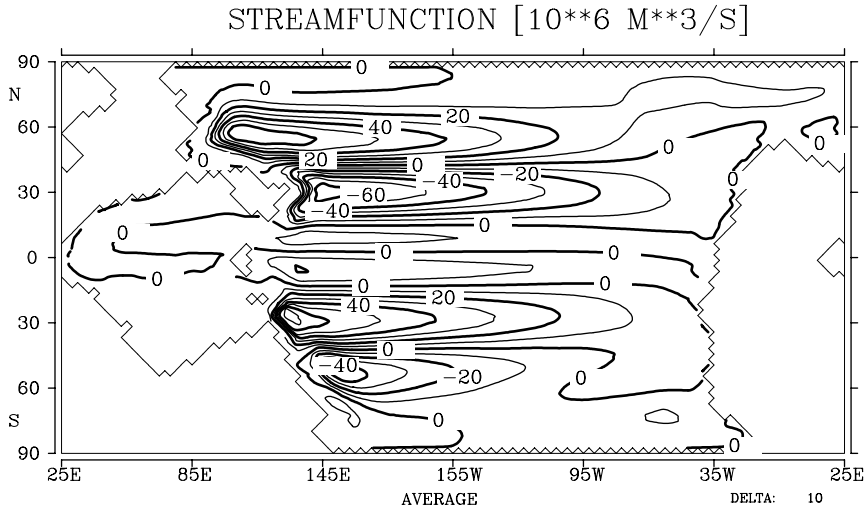

f)

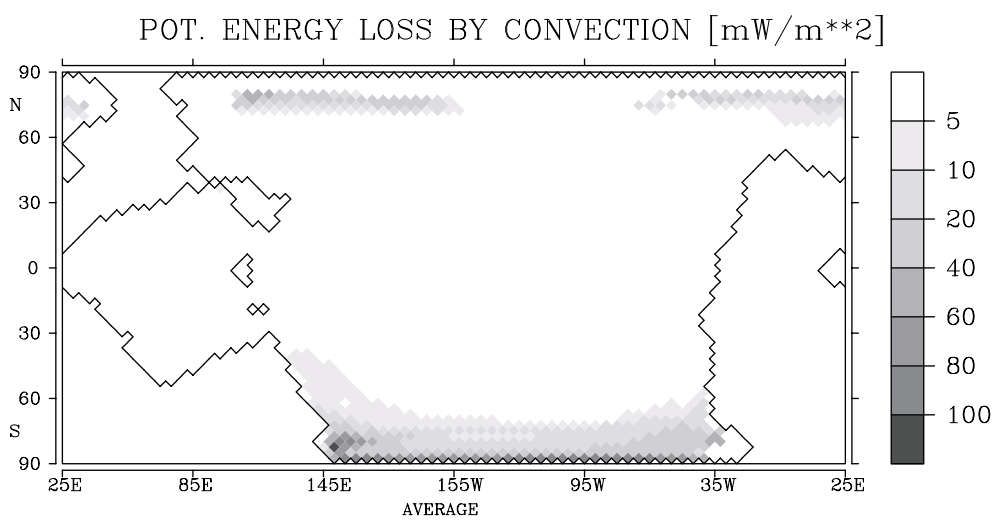

FIGURE 1 (CONTINUED)

AIR SURFACE TEMPERATURE [^{O}C]

a) WORDIAN (4XCO2) LSG/EBM

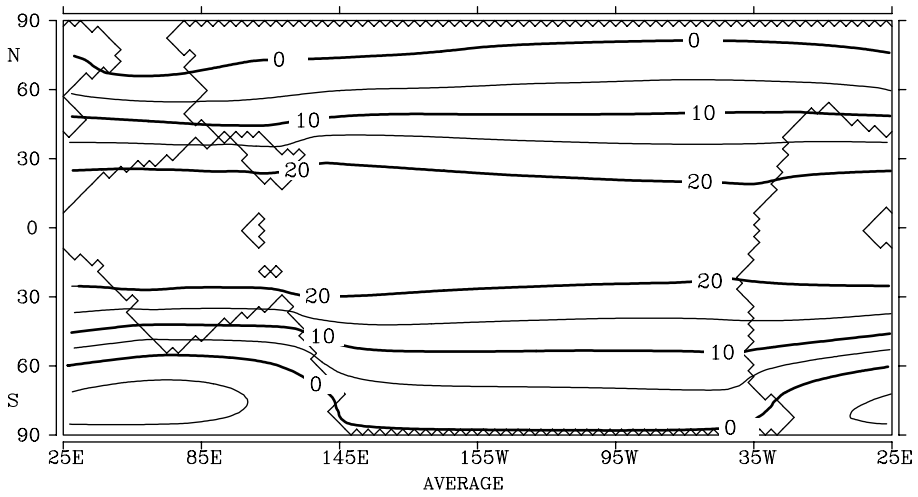

b) WORDIAN (4XCO2) DIFFERENCE GENESIS 2-LSG/EBM

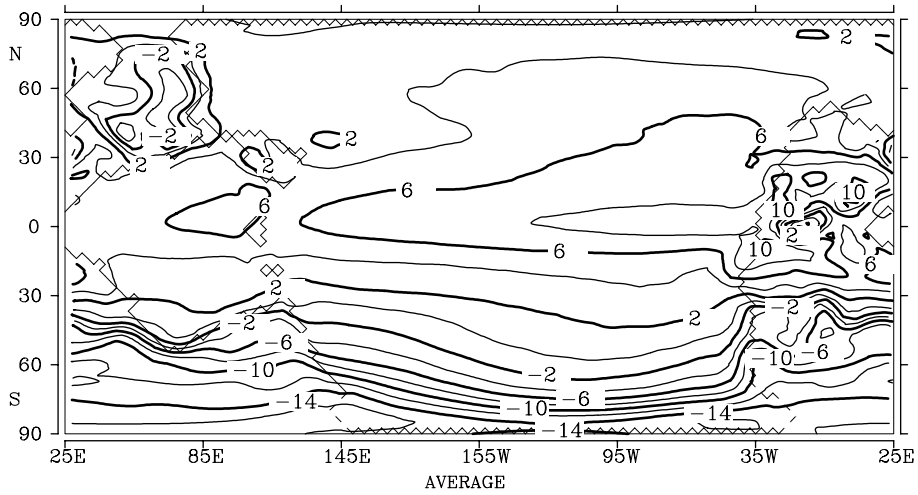

FIGURE 2

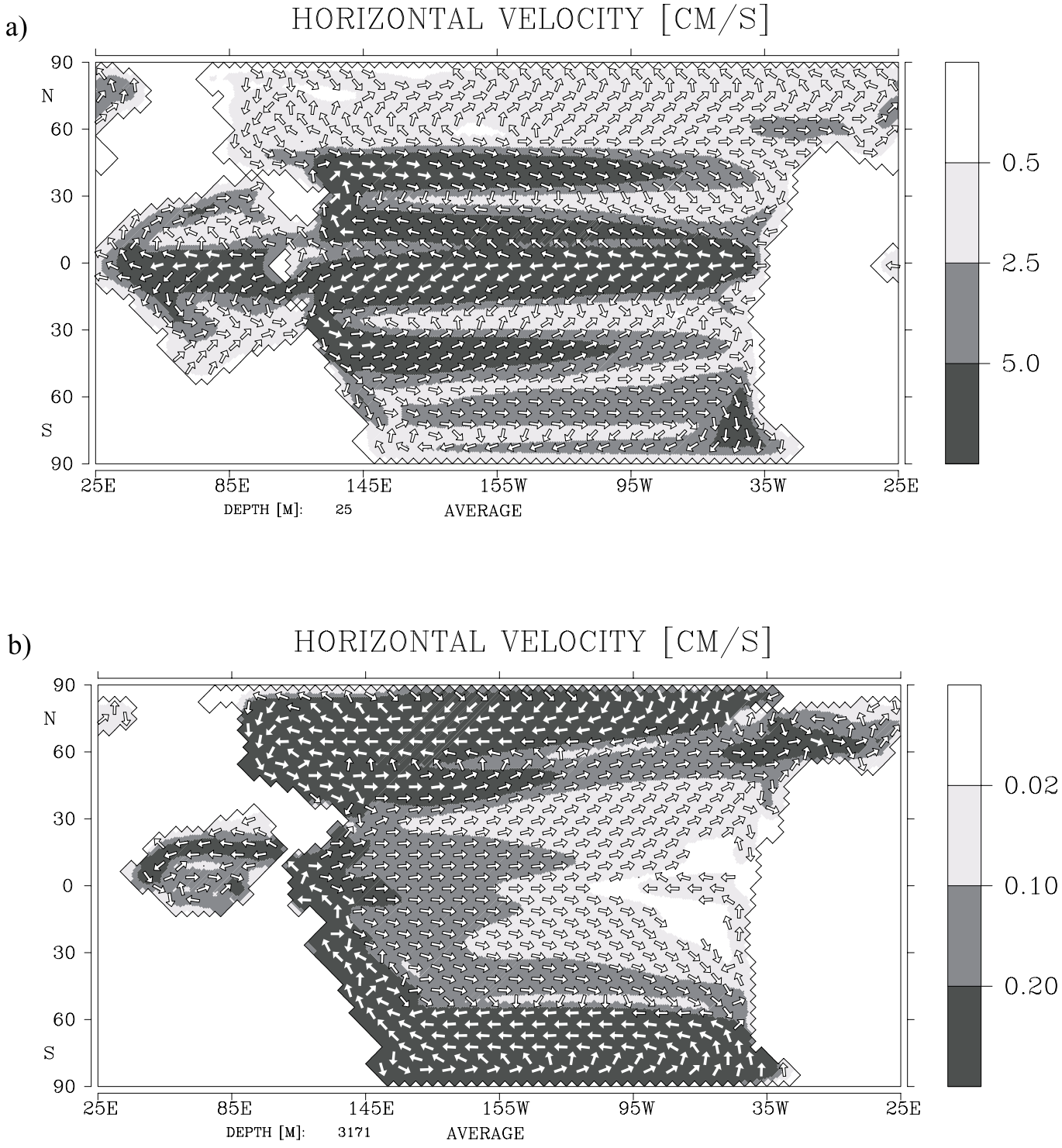
a)
HORIZONTAL VELOCITY [CM/S]
90
N
60
30
0
30
60
S
90
25E
85E
145E
155W
95W
35W
25E
0.5
2.5
5.0
DEPTH [M]: 25
AVERAGE
b)
HORIZONTAL VELOCITY [CM/S]
90
N
60
30
0
30
60
S
90
25E
85E
145E
155W
95W
35W
25E
0.02
0.10
0.20
DEPTH [M]: 3171
AVERAGE

FIGURE 3

WORDIAN (4XCO2) JANUARY

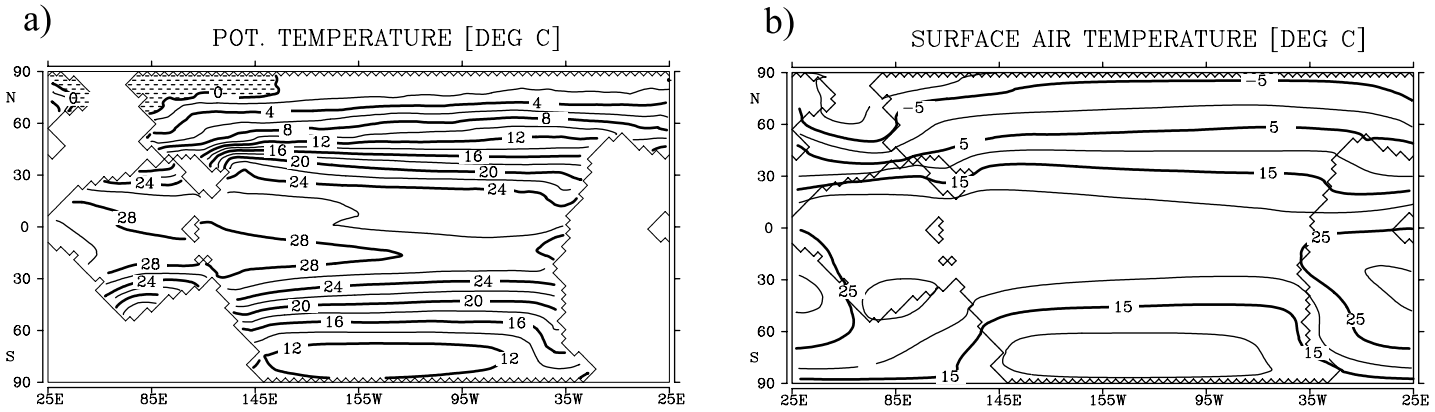

WORDIAN (4XCO2) JULY

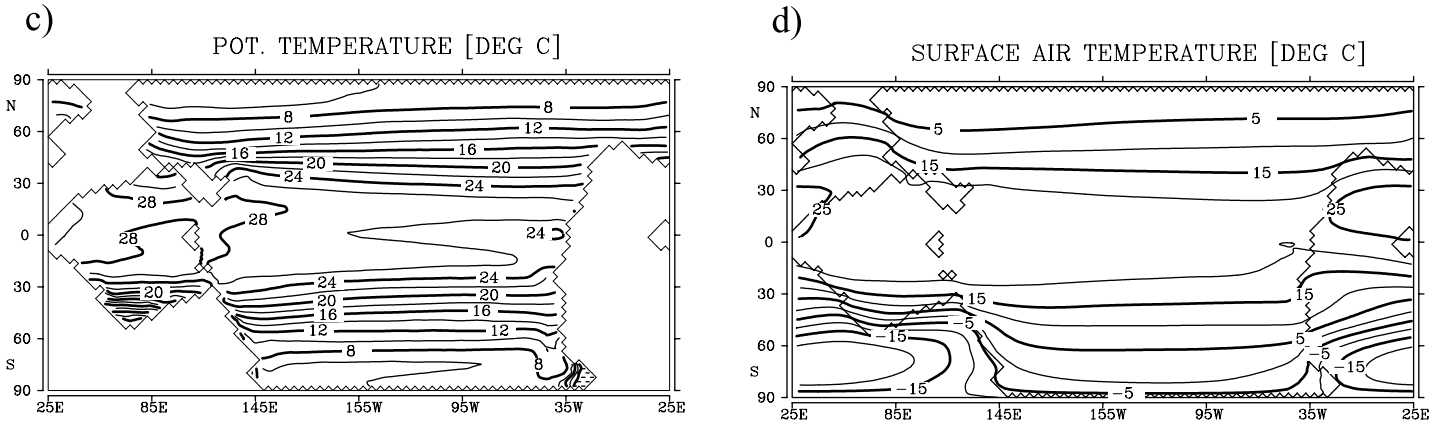

FIGURE 4

WORDIAN (1XCO2)

a)

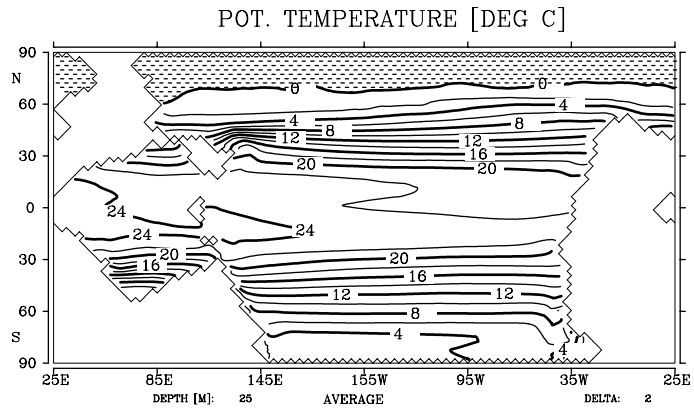

b)

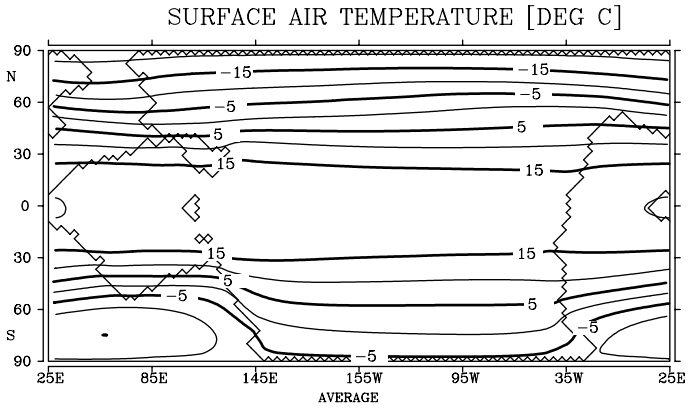

WORDIAN (8XCO2)

c)

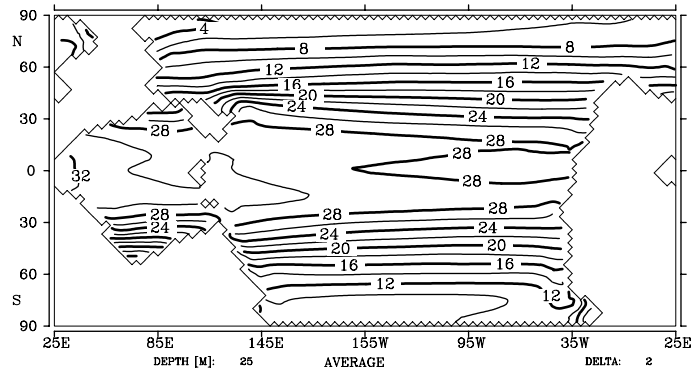

d)

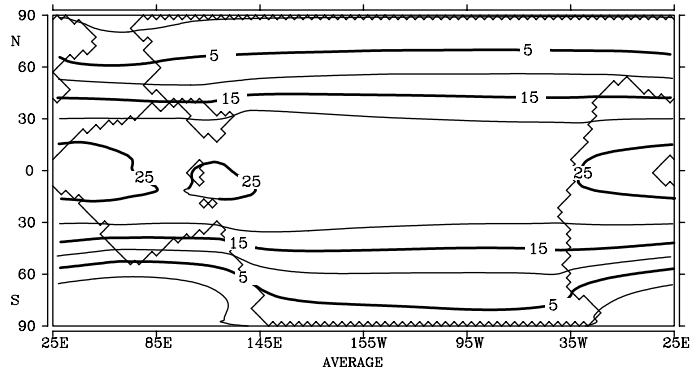

FIGURE 5

ICE THICKNESS [M]

a) WORDIAN (1XCO2)

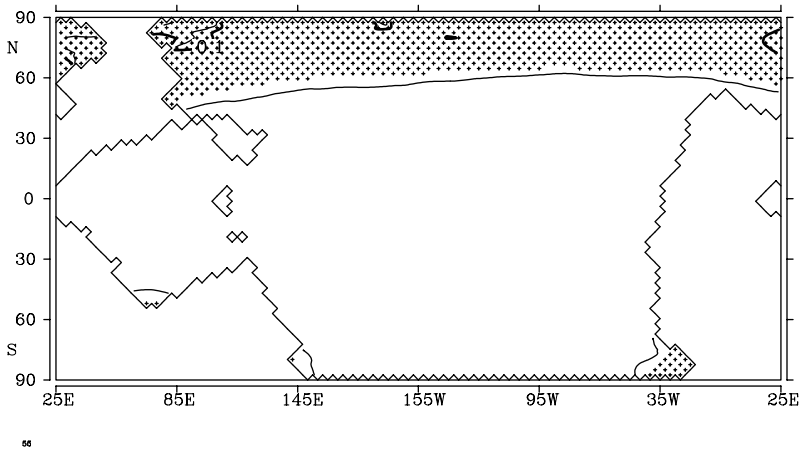

b) WORDIAN (2XCO2)

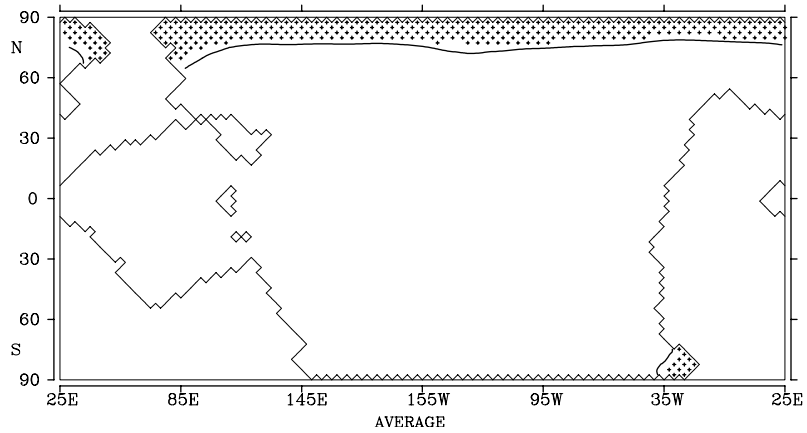

FIGURE 6

a)

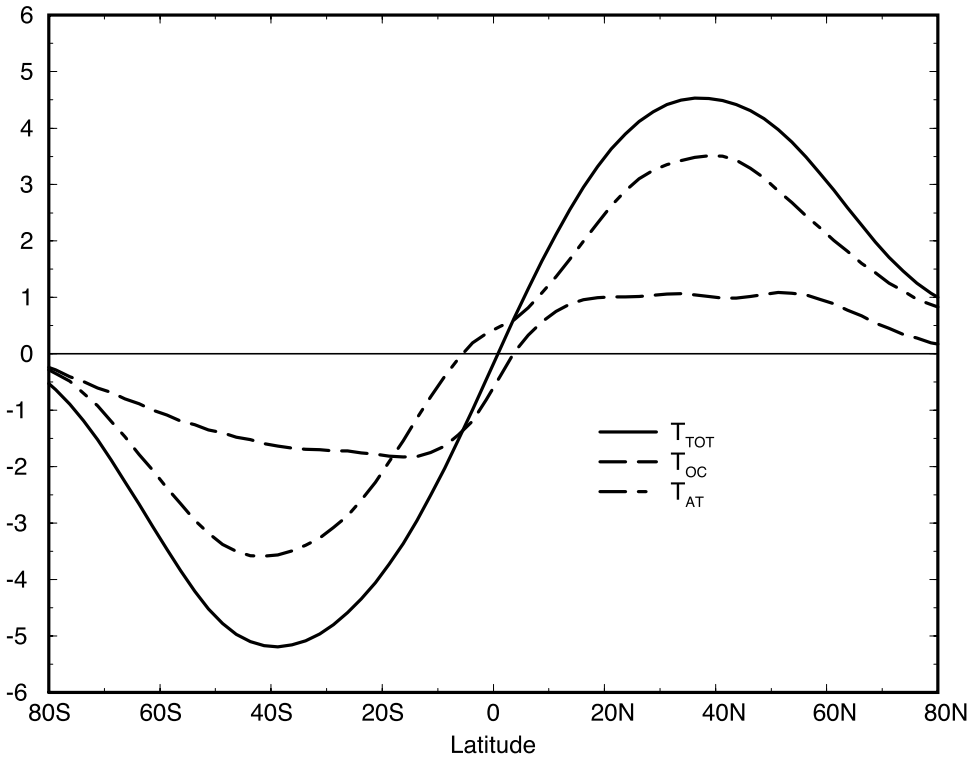
6
5
4
3
2
1
0
-1
-2
-3
-4
-5
-6
80S
60S
40S
20S
0
20N
40N
60N
80N
Latitude
T_{TOT}
T_{OC}
T_{AT}

b)

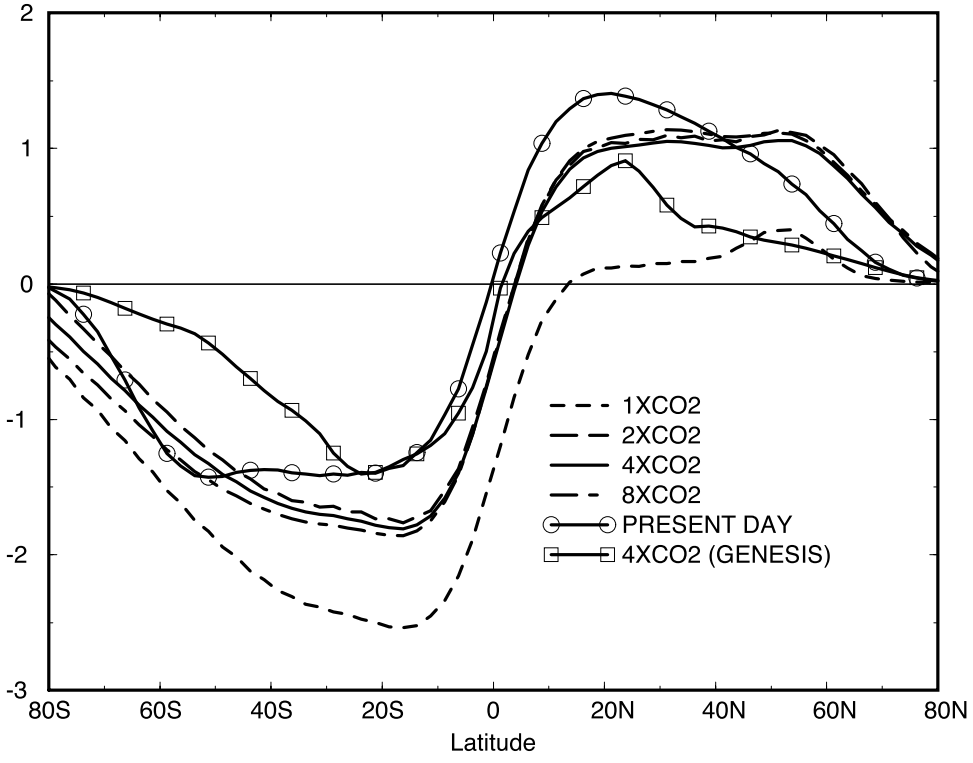
2
1
0
-1
-2
-3
80S
60S
40S
20S
0
20N
40N
60N
80N
Latitude
1XCO2
2XCO2
4XCO2
8XCO2
PRESENT DAY
4XCO2 (GENESIS)

FIGURE 7

MERIDIONAL CIRCULATION [SV]

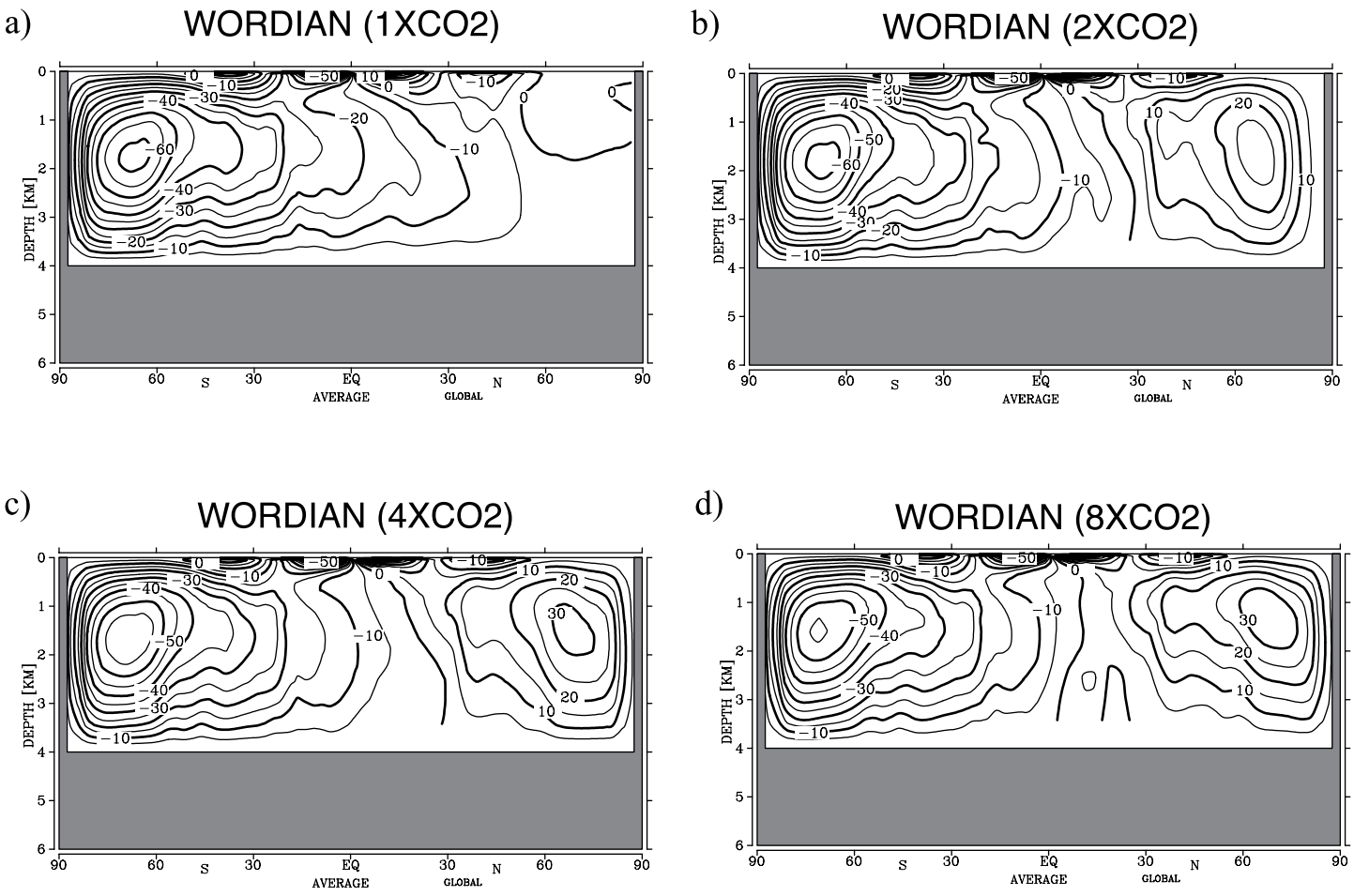

FIGURE 8

a) 4XCO2N-4XCO2 DIFFERENCE IN AIR SURFACE TEMPERATURE [oC]

b) HORIZONTAL VELOCITY [cm/s] 4XCO2N

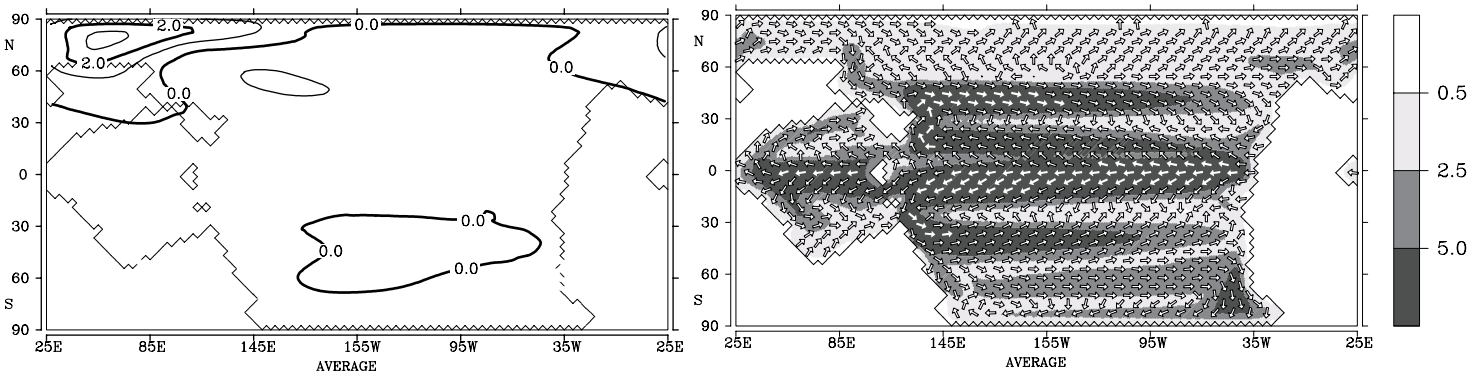

c) 4XCO2S-4XCO2 DIFFERENCE IN AIR SURFACE TEMPERATURE [oC]

d) HORIZONTAL VELOCITY [cm/s] 4XCO2S

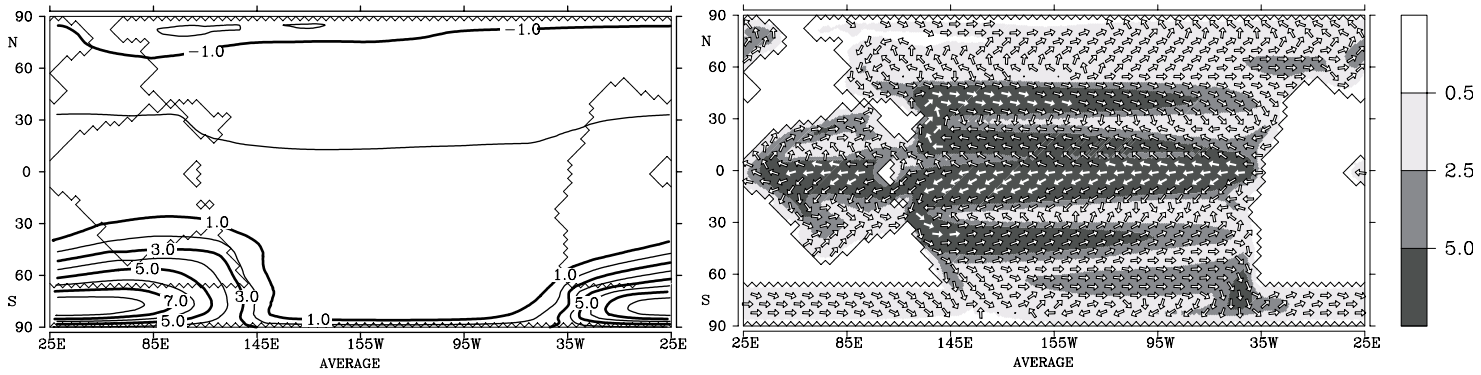

FIGURE 9

Surface Air Temperature [^{o}C]

Hot Summer Orbit - Cold Summer Orbit

a)

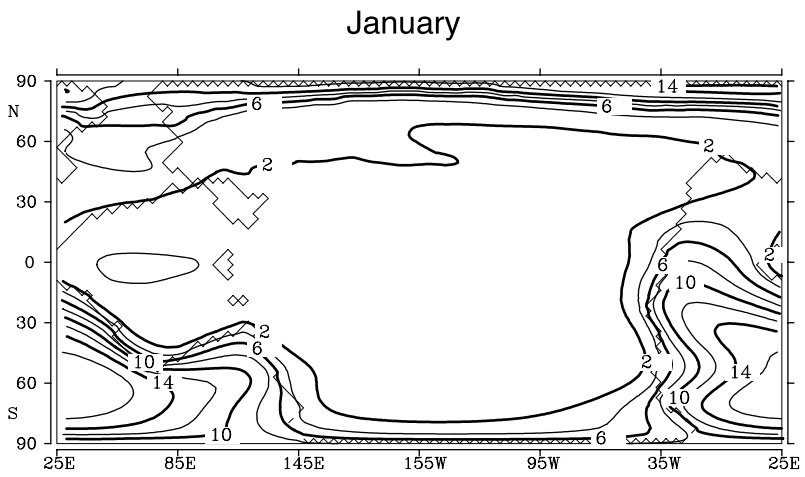

b)

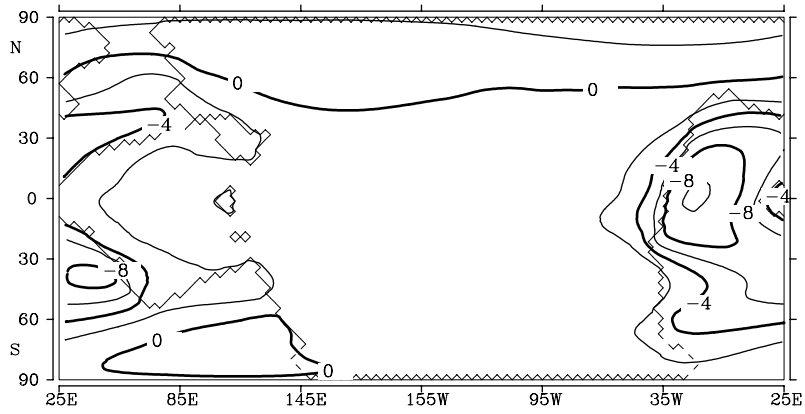

FIGURE 10

a)

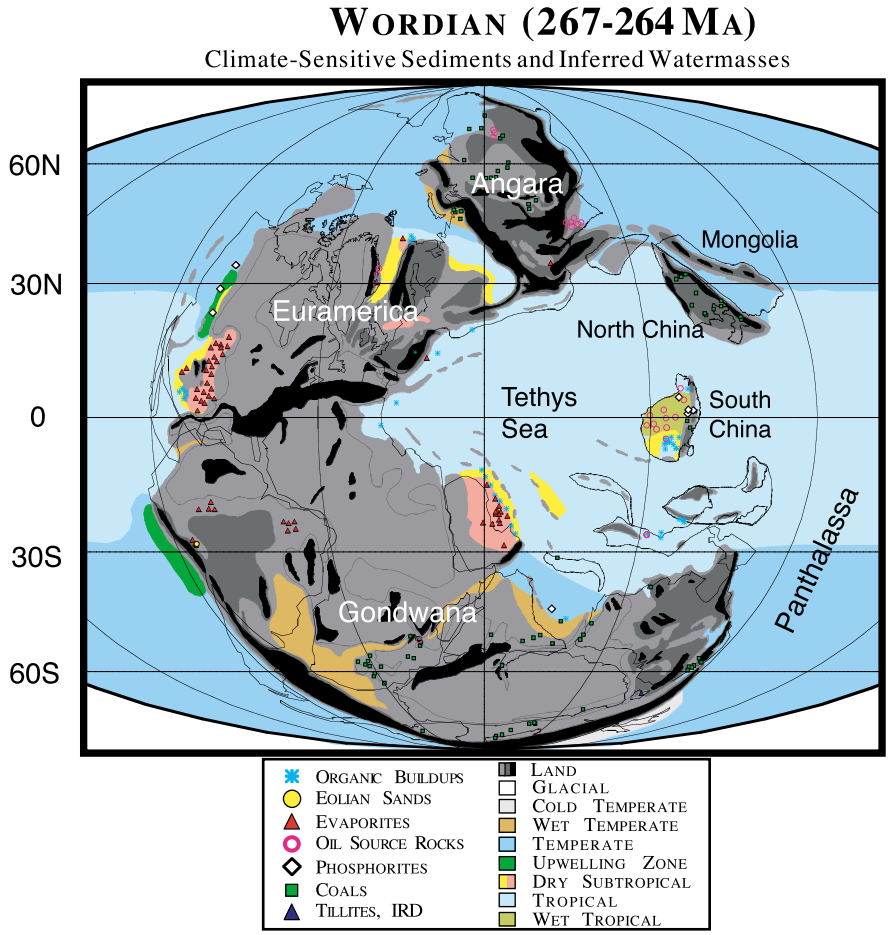
WORDIAN (267-264 MA)
Climate-Sensitive Sediments and Inferred Watermasses
60N
30N
0
30S
60S
Angara
Mongolia
Euramerica
North China
Tethys
Sea
South
China
Panthalassa
Gondwana
ORGANIC BUILDUPS
EOLIAN SANDS
EVAPORITES
OIL SOURCE ROCKS
PHOSPHORITES
COALS
TILLITES, IRD
LAND
GLACIAL
COLD TEMPERATE
WET TEMPERATE
TEMPERATE
UPWELLING ZONE
DRY SUBTROPICAL
TROPICAL
WET TROPICAL

b)

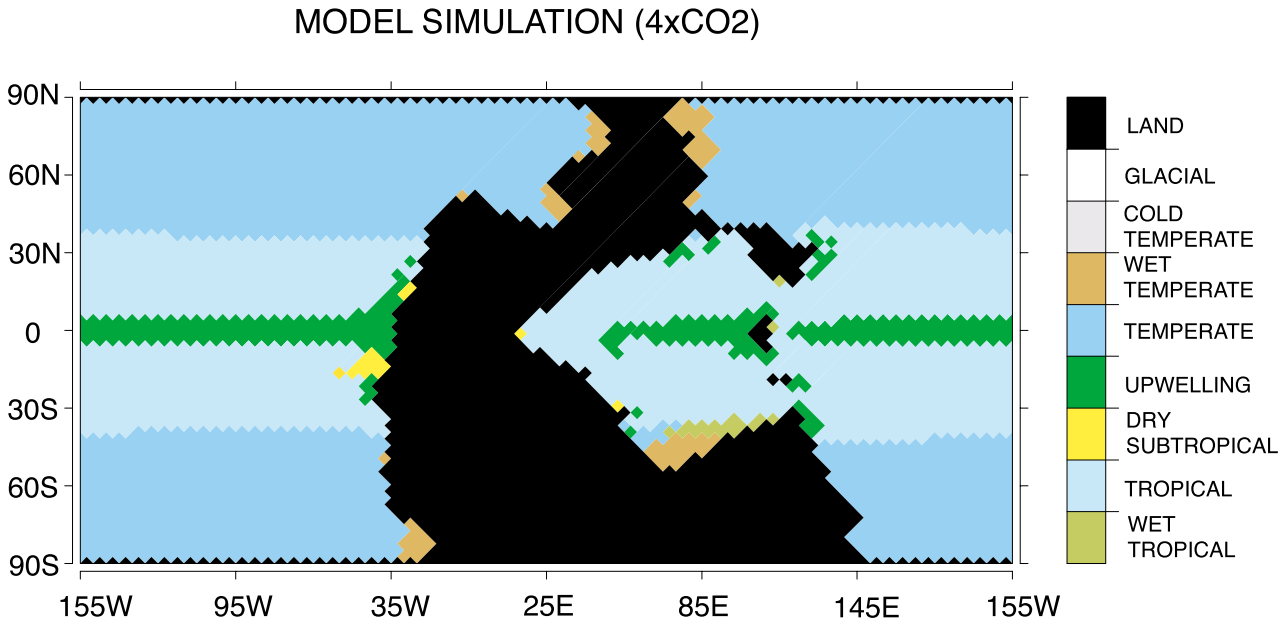
MODEL SIMULATION (4xCO2)
90N
60N
30N
0
30S
60S
90S
155W
95W
35W
25E
85E
145E
155W
LAND
GLACIAL
COLD TEMPERATE
WET TEMPERATE
TEMPERATE
UPWELLING
DRY SUBTROPICAL
TROPICAL
WET TROPICAL

FIGURE 11

MPI-Report-Reference: *Reprinted in

Report 1-276 Please order the reference list from MPI for Meteorology, Hamburg

---

Report No. 277
September 1998

Interannual to Decadal Variability in the Tropical Atlantic
Dietmar Dommenget, Mojib Latif
* Journal of Climate, 1998 (submitted)

Report No. 278
October 1998

Application of a grid-scale lateral discharge model in the BALTEX region
Stefan Hagemann, Lydia Dümenil
* Nordic Hydrology, 30 (3), 209-230, 1999

Report No. 279
October 1998

Cyclostationary Circulation Estimation with a Global Ocean Assimilation System
Detlev Müller, Ralf Giering, Uwe Mikolajewicz, Ernst Maier-Reimer

Report No. 280
October 1998

A coarse grid three dimensional global inverse model of the atmospheric transport
1. Adjoint Model and Jacobian Matrix
2. Inversion of the transport of CO_2 in the 1980s
Thomas Kaminski, Martin Heimann, Ralf Giering
* Journal of Geophysical Research, 1998 (submitted)

Report No. 281
November 1998

Paleonutrient Data Analysis of the Glacial Atlantic using an Adjoint Ocean General Circulation Model
Arne M. E. Winguth, David Archer, Ernst Maier-Reimer, Uwe Mikolajewicz
* AGU Geophysical Monograph Series, Vol. 114, 171-183, 1999

Report No. 282
November 1998

The Effect of Environmental Conditions on Volcanic Plume Rise
Hans-F. Graf, Michael Herzog, Josef M. Oberhuber, Christiane Textor
* Journal of Geophysical Research, 1998 (submitted)

Report No. 283
December 1998

Model Simulations of the Changing Distribution of Ozone and its Radiative Forcing of Climate:
Past, Present and Future
Geert-Jan Roelofs, Jos Lelieveld, Johann Feichter

Report No. 284
December 1998

Predicting the Number of Cloud Droplets in the ECHAM GCM
Ulrike Lohmann, Johann Feichter, Catherine C. Chuang, Joyce E. Penner
* Journal of Geophysical Research - Atmospheres, 1998 (accepted)

Report No. 285
December 1998

The Role of Ocean Dynamics for Low-Frequency Fluctuations of the NAO in a Coupled Ocean-Atmosphere GCM
Michael Christoph, Uwe Ulbrich, Josef M. Oberhuber, Erich Roeckner

Report No. 286
January 1999

Formation of nitrous acid: Parameterisation and comparison with observations
Gerhard Lammel

Report No. 287
Februar 1999

Natürliche Senken und Quellen des atmosphärischen Kohlendioxids: Stand des Wissens und Optionen des Handelns
Martin Heimann, Christine Weber, Jan C. Duinker, Arne Körtzinger, Ludger Mintrop, Nina Buchmann, Ernst-Detlef Schulze, Michaela Hein, Alberte Bondeau, Wolfgang Cramer, Marcus Lindner, Gerd Esser

Report No. 288
March 1999

Large-eddy simulation of a nocturnal stratocumulus-topped marine atmospheric boundary layer:
An uncertainty analysis
Andreas Chlond, Andreas Wolkau
Boundary-Layer Meteorology, 1999 (submitted)

Report No. 289
March 1999

Derivation of global GCM boundary conditions from 1 km land use satellite data
Stefan Hagemann, Michael Botzet, Lydia Dümenil, Bennert Machenhauer

Report No. 290
June 1999
A nonlinear impulse response model of the coupled carbon cycle-ocean-atmosphere climate system
Georg Hooss, Reinhard Voss, Klaus Hasselmann, Ernst Maier-Reimer, Fortunat Joos

Report No. 291
June 1999
Rapid algorithms for plane-parallel radiative transfer calculations
Vassili Prigarin

Report No. 292
June 1999
Oceanic Control of Decadal North Atlantic Sea Level Pressure Variability in Winter
Mojib Latif, Klaus Arpe, Erich Roeckner
* Geophysical Research Letters, 1999 (submitted)

Report No. 293
July 1999
A process-based, climate-sensitive model to derive methane emissions from natural wetlands: Application to 5 wetland sites, sensitivity to model parameters and climate
Bernadette P. Walter, Martin Heimann
* Global Biogeochemical Cycles, 1999 (submitted)

Report No. 294
August 1999
Possible Changes of $\delta^{18}O$ in Precipitation Caused by a Meltwater Event in the North Atlantic
Martin Werner, Uwe Mikolajewicz, Georg Hoffmann, Martin Heimann
* Journal of Geophysical Research - Atmospheres, 105, D8, 10161-10167, 2000

Report No. 295
August 1999
Borehole versus Isotope Temperatures on Greenland: Seasonality Does Matter
Martin Werner, Uwe Mikolajewicz, Martin Heimann, Georg Hoffmann
* Geophysical Research Letters, 27, 5, 723-726, 2000

Report No. 296
August 1999
Numerical Modelling of Regional Scale Transport and Photochemistry directly together with Meteorological Processes
Bärbel Langmann
* Atmospheric Environment, 34, 3585-3598, 2000

Report No. 297
August 1999
The impact of two different land-surface coupling techniques in a single column version of the ECHAM4 atmospheric model
Jan-Peter Schulz, Lydia Dümenil, Jan Polcher
* Journal of Applied Meteorology, 40, 642-663, 2001

Report No. 298
September 1999
Long-term climate changes due to increased CO_2 concentration in the coupled atmosphere-ocean general circulation model ECHAM3/LSG
Reinhard Voss, Uwe Mikolajewicz
* Climate Dynamics, 17, 45-60, 2000

Report No. 299
October 1999
Tropical Stabilisation of the Thermohaline Circulation in a Greenhouse Warming Simulation
Mojib Latif, Erich Roeckner
* Journal of Climate, 1999 (submitted)

Report No. 300
October 1999
Impact of Global Warming on the Asian Winter Monsoon in a Coupled GCM
Zeng-Zhen Hu, Lennart Bengtsson, Klaus Arpe
* Journal of Geophysical Research-Atmosphere, 105, 4607-4624, 2000

Report No. 301
December 1999
Impacts of Deforestation and Afforestation in the Mediterranean Region as Simulated by the MPI Atmospheric GCM
Lydia Dümenil Gates, Stefan Ließ

Report No. 302
December 1999
Dynamical and Cloud-Radiation Feedbacks in El Niño and Greenhouse Warming
Fei-Fei Jin, Zeng-Zhen Hu, Mojib Latif, Lennart Bengtsson, Erich Roeckner
* Geophysical Research Letter, 28, 8, 1539-1542, 2001

Report No. 303
December 1999
The leading variability mode of the coupled troposphere-stratosphere winter circulation in different climate regimes
Judith Perlwitz, Hans-F. Graf, Reinhard Voss
* Journal of Geophysical Research, 105, 6915-6926, 2000

Report No. 304
January 2000
Generation of SST anomalies in the midlatitudes
Dietmar Dommenget, Mojib Latif
* Journal of Climate, 1999 (submitted)

Report No. 305
June 2000
Tropical Pacific/Atlantic Ocean Interactions at Multi-Decadal Time Scales
Mojib Latif
* Geophysical Research Letters, 2000 (submitted)

Report No. 306
June 2000
On the Interpretation of Climate Change in the Tropical Pacific
Mojib Latif
* Journal of Climate, 2000 (submitted)

Report No. 307
June 2000
Observed historical discharge data from major rivers for climate model validation
Lydia Dümenil Gates, Stefan Hagemann, Claudia Golz

Report No. 308
July 2000
Atmospheric Correction of Colour Images of Case I Waters - a Review of Case II Waters - a Review
D. Pozdnyakov, S. Bakan, H. Grassl
* Remote Sensing of Environment, 2000 (submitted)

Report No. 309
August 2000
A Cautionary Note on the Interpretation of EOFs
Dietmar Dommenget, Mojib Latif
* Journal of Climate, 2000 (submitted)

Report No. 310
September 2000
Midlatitude Forcing Mechanisms for Glacier Mass Balance Investigated Using General Circulation Models
Bernhard K. Reichert, Lennart Bengtsson, Johannes Oerlemans
* Journal of Climate, 2000 (accepted)

Report No. 311
October 2000
The impact of a downslope water-transport parameterization in a global ocean general circulation model
Stephanie Legutke, Ernst Maier-Reimer

Report No. 312
November 2000
The Hamburg Ocean-Atmosphere Parameters and Fluxes from Satellite Data (HOAPS): A Climatological Atlas of Satellite-Derived Air-Sea-Interaction Parameters over the Oceans
Hartmut Graßl, Volker Jost, Ramesh Kumar, Jörg Schulz, Peter Bauer, Peter Schlüssel

Report No. 313
December 2000
Secular trends in daily precipitation characteristics: greenhouse gas simulation with a coupled AOGCM
Vladimir Semenov, Lennart Bengtsson

Report No. 314
December 2000
Estimation of the error due to operator splitting for micro-physical-multiphase chemical systems in meso-scale air quality models
Frank Müller
* Atmospheric Environment, 2000 (submitted)

Report No. 315
January 2001
Sensitivity of global climate to the detrimental impact of smoke on rain clouds
Hans-F. Graf, Daniel Rosenfeld, Frank J. Nober
* nur unter www.mpimet.mpg.de · Veröffentlichungen · MPI-Reports

Report No. 316 March 2001	**Lake Parameterization for Climate Models** Ben-Jei Tsuang, Chia-Ying Tu, Klaus Arpe
Report No 317 March 2001	**The German Aerosol Lidar Network:** **Methodology, Data, Analysis** J. Bösenberg, M. Alpers, D. Althausen, A. Ansmann, C. Böckmann, R. Eixmann, A. Franke, V. Freudenthaler, H. Giehl, H. Jäger, S. Kreipl, H. Linné, V. Matthias, I. Mattis, D. Müller, J. Sarközi, L. Schneidenbach, J. Schneider, T. Trickl, E. Vorobieva, U. Wandinger, M. Wiegner
Report No. 318 March 2001	**On North Pacific Climate Variability** Mojib Latif * Journal of Climate, 2001 (submitted)
Report No. 319 March 2001	**The Madden-Julian Oscillation in the ECHAM4 / OPYC3 CGCM** Stefan Liess, Lennart Bengtsson, Klaus Arpe * Climate Dynamics, 2001 (submitted)
Report No. 320 May 2001	**Simulated Warm Polar Currents during the Middle Permian** A. M. E. Winguth, C. Heinze, J. E. Kutzbach, E. Maier-Reimer, U. Mikolajewicz, D. Rowley, A. Rees, A. M. Ziegler * Paleoceanography, 2001 (submitted)

ISSN 0937-1060